

# Bidirectional Reflectance Round-Robin in Support of the Earth Observing System Program

E. A. Early, P. Y. Barnes, and B. C. Johnson  
Optical Technology Division  
National Institute of Standards and Technology  
Gaithersburg, MD 20899

J. J. Butler  
Space Geodesy Networks and Sensor Calibration Office, Code 920.1  
Goddard Space Flight Center  
National Aeronautics and Space Administration  
Greenbelt, MD 20771

C. J. Bruegge  
Jet Propulsion Laboratory  
California Institute of Technology  
Pasadena, CA 91109

S. F. Biggar and P. R. Spyak  
Remote Sensing Group, Optical Sciences Center  
University of Arizona  
Tucson, AZ 85721

M. M. Pavlov  
Raytheon Santa Barbara Remote Sensing  
Goleta, CA 93117

## **Abstract**

Laboratory measurements of the bidirectional reflectance distribution function (BRDF) of diffuse reflectors are required to support calibration in the Earth Observing System (EOS) program of the National Aeronautics and Space Administration. To assess the ability of the instrument calibration laboratories to perform accurate BRDF measurements, a round-robin with the National Institute of Standards and Technology (NIST) as the central laboratory was initiated by the EOS Project Science Office. The round-robin parameters include sample type, wavelength, and incident and viewing

angles. The results show that the participating calibration laboratories are, with a few exceptions due to experimental techniques or sample properties, generally able to measure BRDF for the round-robin parameters to within 2 % of the values measured by NIST.

Key Words: aluminum; BRDF; EOS; PTFE; reflectance; round-robin; Spectralon

## **I. Introduction**

Some optical sensors in the Earth Observing System (EOS) program require an accurate determination of the bidirectional reflectance distribution function (BRDF) of diffusely reflecting samples. Determining the BRDF of these samples is needed for establishing a standard of spectral radiance using a source of known spectral irradiance or for establishing a standard of BRDF for determining the Earth's BRDF from ratio measurements. For example, integrating sphere sources used to determine the spectral radiance responsivity of optical sensors prior to deployment can be calibrated using a lamp standard of spectral irradiance and a diffuse reflector. During deployment of the optical sensor on-orbit, solar illumination of a diffuse reflector provides a source of spectral radiance if the solar irradiance is known. Alternatively, the ratio of solar-reflected signals from the Earth and the diffuse reflector can be used to derive the Earth's reflectance. In the EOS program, these types of measurements may be used for optical sensors on spacecraft (such as the EOS AM-1 platform), or for radiometric calibration of sensors on aircraft or on the ground.

As a verification of the BRDF measurements related to EOS, the EOS Project Science Office and the National Institute of Standards and Technology (NIST) designed a round-robin experiment with four types of diffuse reflectors among five different laboratories (Butler 1996a, Butler 1996b). Preliminary results have been reported at optical radiometry conferences (Johnson 1998b, Barnes 1998); this paper reports the final, complete results of the round-robin.

Previous comparisons of the BRDF of diffusely and specularly reflecting samples have often indicated a variability that is greater than the uncertainties in the BRDF measurements assigned by the individual laboratories (Leonard 1988, Jaross 1998). Systematic effects that can compromise BRDF measurements include scattered light, sample uniformity, polarization effects, alignment, measurement geometry, and calibration methods. Comparisons between laboratories of the BRDF of a common set of samples evaluate the complete measurement procedures, and are therefore essential to identify any biases and to establish confidence in the uncertainties assigned by the laboratories.

The central facility in the EOS BRDF round-robin is the Spectral Tri-function Automated Reference Reflectometer (STARR) at NIST (Proctor 1996, Barnes 1998a), with measurements alternating between NIST and the other laboratories. The participating laboratories are the Goddard Space Flight Center (GSFC) of the National Aeronautics and Space Administration (NASA), the Jet Propulsion Laboratory (JPL) of the California Institute of Technology, Raytheon Santa Barbara Remote Sensing (SBRs), and the Remote Sensing Group of the Optical Sciences Center at the University of Arizona (UA). These laboratories support, respectively, various spacecraft programs

(Schiff 1993), the Multiangle Imaging Spectroradiometer (MISR) (Diner 1998), the Moderate-Resolution Imaging Spectroradiometer (MODIS) (Guenther 1996), and surface-based land reflectance experiments (Slater 1996).

The next section details the experimental procedures used for this round-robin, particularly the experimental protocol and the measurement techniques used by the participating laboratories. The following section on the results is divided into three subsections, one on the BRDF properties of the samples, the next on the results of the NIST measurements, and the last on the agreement between the BRDF values measured by the participants and those measured by NIST.

## II. Experimental Procedure

The BRDF is the fundamental quantity describing the reflectance properties of a sample (Nicodemus 1977). It is denoted by  $f_r$  and is given by

$$f_r(\theta_i, \phi_i; \theta_v, \phi_v; \lambda) = \frac{dL_r(\theta_i, \phi_i; \theta_v, \phi_v; \lambda)}{dE_i(\theta_i, \phi_i; \lambda)},$$

where  $dL_r$  is the reflected radiance,  $dE_i$  is the incident irradiance,  $\theta$  is the polar angle,  $\phi$  is the azimuthal angle, the subscripts i and v refer to the incident and viewed directions, and  $\lambda$  is the wavelength. The absolute method for determining  $f_r$  of a sample requires measurements of both  $dL_r$  and  $dE_i$  using a spectroradiometer (ASTM 1997). The source illuminates the sample from the  $\theta_i, \phi_i$  direction and the reflected radiance  $dL_r$  is measured in the  $\theta_v, \phi_v$  direction. Using the same detector, the incident irradiance  $dE_i$  is also measured. Alternative relative determinations of  $f_r$  involve normalizations other than to the incident irradiance and require additional information, such as the total hemispherical

reflectance, the BRDF of a diffuse reflectance standard, or the specular reflectance of a standard (ASTM 1997).

The experimental protocol for the EOS BRDF round-robin was determined after consultation with all the participants. The samples, wavelengths, incident and viewing angles, and measurement conditions were chosen both by their importance to the EOS program and by the capabilities of the participants. The experimental protocol parameters are given in Table 1.

A set of four samples was used for the round-robin measurements. The first sample was Spectralon from Labsphere, Inc.\* The next two samples were made by NIST using Type F5 polytetrafluoroethylene (PTFE) powder from Aussimont with a 25  $\mu\text{m}$  particle size. Both samples were pressed to a density of 1  $\text{g}/\text{cm}^3$  and the surface was imprinted with 180 grit sandpaper, and one was further sintered at 360  $^{\circ}\text{C}$  for one hour, with a 3  $^{\circ}\text{C}/\text{min}$  heating and cooling rate. These samples are referred to as pressed PTFE and sintered PTFE. The fourth sample was vacuum-deposited aluminum on a ground-aluminum surface, acquired from Ball Aerospace. The four samples were designated by letter for the round-robin – A for Spectralon, B for pressed PTFE, C for sintered PTFE, and D for aluminum. These samples were chosen because they are representative of standards used for diffuse reflectance. Spectralon is a very common reflectance standard because it can be machined and is durable, while pressed PTFE is used as the reflectance standard at NIST (Weidner 1981). Sintered PTFE was included in the set to afford comparison with the pressed PTFE, while aluminum has been used occasionally as a

---

\* Certain commercial equipment, instruments, or materials are identified in this paper to foster understanding. Such identification does not imply recommendation or endorsement by the National Institute of Standards and Technology, nor does it imply that the materials or equipment identified are necessarily the best available for the purpose.

reflectance standard (Park 1996) and has different optical properties than the other samples. In addition, the samples had different scattering mechanisms. The Spectralon and pressed PTFE scatter from the bulk, aluminum scatters from the surface, and sintered PTFE scatters from both the bulk and the surface.

The wavelengths were chosen to correspond with those used on EOS optical sensors or with laser lines, and the angles covered the ranges usually encountered with EOS measurements of BRDF. While the participants agreed on the wavelengths and angles specified by the protocol, most were not able to measure at these values due to the capabilities of their instruments. As detailed in the next section, this did not significantly affect the BRDF comparison results. All measurements were in-plane ( $\phi_i = \phi_v = 0$ ) and reported for unpolarized radiant flux. While BRDF depends on polarization, some participants were not able to measure with different polarizations and the BRDF applications for the EOS optical sensors generally use unpolarized light. For those participants that were able to measure BRDF for different polarization states, the BRDF for unpolarized radiant flux was obtained by appropriately averaging the BRDFs for polarized light. The angular and polarization conventions, and the orientation of the fiducial mark on the sample, are shown in Fig. 1. The incident angle  $\theta_i$  and viewing angle  $\theta_v$  are measured from the normal of the sample. Both angles are positive in Fig. 1. and therefore  $\theta_v = -\theta_i$  for specular reflection.

The samples were shipped in an optical-quality metal case with a one-way pressure relief valve that provided pressure equilibrium at high altitudes in the aircraft baggage compartment but prevented intake of any contaminated air for the remainder of the transport. The pressure was equalized once the case was inside the laboratory facility,

which was usually a clean room. The shipment included a set of handling and measurement instructions. Prior to the measurements, the participants were asked to supply information on their instrumentation and techniques, and they were provided with mechanical drawings of the samples and instructions on the data format. A timetable of the measurements by the participants is given in Table 2.

Data files in a common format containing the results from each participating laboratory were provided to NIST for analysis. The BRDF and its standard uncertainty as a function of viewing angle are listed in a data file for each participant, sample, wavelength, and incident angle. Descriptive data that includes the measurement parameters and other important information precedes the BRDF data.

The STARR instrument at NIST is absolute – the incident and reflected fluxes are measured, along with the polar viewing angle and solid angle of the receiver (Proctor 1996). The source consists of xenon-arc or quartz-tungsten-halogen lamps, a monochromator, a Glan-Taylor polarizer, and associated optical components. The receiver has a precision aperture, a focusing lens, and Si, Ge, or InAs photodiodes. The STARR goniometer consists of the sample holder and the receiver, and the measurement geometry is in-plane.

The instrument at GSFC is designed to measure bidirectional reflectance using lasers or a xenon-arc lamp and monochromator (Schiff 1993). In- or out-of-plane measurements are made either relative to a BRDF standard or in an absolute manner. For the work reported here, absolute measurements were performed using the monochromator as the source and a Si photodiode as the detector. For measurements in

the ultraviolet (required for atmospheric-ozone programs at GSFC), a photomultiplier tube can also be used.

Although absolute bidirectional reflectance measurements were made at JPL for this EOS comparison, MISR has no requirement on the absolute accuracy of BRDF values. Rather, the requirement is to provide normalized (or relative) BRDF values, which are the ratio of the bidirectional reflectance at the viewing angle of a given MISR camera to that at the viewing angle of the MISR on-board detector standard (Diner 1998). The JPL instrument developed for MISR uses three lasers at wavelengths of 442 nm, 632.8 nm, and 859.9 nm (McGuckin 1996). Beam-expanding telescopes with spatial filters produce collimated light on the sample. The receiver has a telescope, a Si photodiode, and associated electronics. The receiver can be rotated around the sample, and the sample can be tilted for out-of-plane measurements. A separate detector system monitors the stability of the source.

The SBRS scattering goniometer uses a Spectralon sample as a standard of bidirectional reflectance (Wells 1994). This standard was calibrated by NIST using the STARR instrument. The SBRS technique accounts for the effect of depolarization upon scattering (Clarke 1983), and uses a Wollaston polarizer in the receiver assembly for simultaneous measurements of *p*- and *s*-polarized reflected radiant flux. The source consists of a quartz-tungsten-halogen lamp, bandpass filters, a Glan-Thompson prism, focusing lenses, apertures, and baffles. Depending on the wavelength, the detector is a photomultiplier tube or Ge or InSb photodiode.

The UA technique uses a pressed PTFE sample as a standard of hemispherical reflectance (Spyak 1997); the preparation procedure and reflectance values are derived

from NIST and ASTM (American Society for Testing and Materials) publications. The source is a constant-current-controlled, quartz-tungsten-halogen lamp. The receiver consisted of imaging optics, interference filters, and a Si photodiode. The sample and receiver are rotated to provide a range of incident and viewing angles (Biggar 1988).

### III. Results and Discussion

#### A. BRDF Properties of Samples

The BRDF of each sample is a function of incident angle  $\theta_i$ , viewing angle  $\theta_v$ , and wavelength  $\lambda$ , so that  $f_r = f_r(\theta_i, \theta_v, \lambda)$ . The dependence of  $f_r$  on these three parameters is important for understanding the results obtained by NIST and the participants, and is therefore the topic of this section. This dependence is based on the average BRDFs obtained from the NIST measurements, detailed in the next section.

Since the BRDF of a sample is a function of three parameters,  $\theta_i$ ,  $\theta_v$ , and  $\lambda$ , it thus presents a challenge for showing these dependencies in two-dimensional plots. A useful approach is to plot BRDF as a function of viewing angle,  $f_r(\theta_v)$ , for each sample, incident angle, and wavelength, as shown in Figs. 2 to 5. Wavelengths of 1240 nm and 1700 nm are not included in any of the results since they were each measured by only one laboratory, NIST and SBRs, respectively. Note the difference in the vertical scale for the (d) panels as compared to the other panels in each figure.

Figures 2 to 5 demonstrate that the BRDF of the samples depends strongly on the incident and viewing angles and weakly on wavelength. For the incident angle dependence,  $f_r(\theta_v)$  increases dramatically towards the specular direction ( $\theta_v = -\theta_i$ ) with increasing  $\theta_i$ . This effect becomes increasingly pronounced from Spectralon to pressed

PTFE to sintered PTFE to aluminum. For the wavelength dependence,  $f_r(\theta_v)$  for  $\theta_i = 0^\circ$  generally increases slightly with increasing  $\lambda$  for all the samples. For  $\theta_i \neq 0^\circ$ ,  $f_r(\theta_v)$  generally increases (decreases) with  $\lambda$  for negative (positive)  $\theta_v$ , although this dependence is not as pronounced for sintered PTFE as it is for the other samples. Note especially that the BRDF can deviate substantially from its ideal value of  $1/\pi \text{ sr}^{-1}$  ( $0.3183 \text{ sr}^{-1}$ ), illustrating the departure of the reflecting properties from those of an ideal diffuse reflector.

Two other plots show subsets of the results presented in Figs. 2 to 5, and are useful for understanding the BRDF properties of the samples. The BRDF as a function of wavelength for each sample is shown in Fig. 6 at two different bidirectional angle combinations. A bidirectional angle combination often used for measuring diffuse reflectance is used for Fig. 6(a). For Spectralon and pressed and sintered PTFE,  $f_r(\lambda)$  is nearly constant with  $\lambda$ , and is slightly lower for sintered PTFE than it is for the other two samples. For aluminum,  $f_r(\lambda)$  is lower than for the other samples and has the expected spectral shape for this metal (Barnes 1998a). At the other extreme, the bidirectional angle combination for demonstrating specular reflectance is used for Fig. 6(b). For all samples,  $f_r(\lambda)$  increases with  $\lambda$ , and now  $f_r(\lambda)$  for sintered PTFE and aluminum is greater than that for Spectralon and pressed PTFE. Finally, the BRDF as a function of viewing angle at a wavelength of 633 nm is shown in Fig. 7 for each sample and incident angle, and the ideal value of  $1/\pi \text{ sr}^{-1}$  is shown as a horizontal line. This figure demonstrates the dramatic changes that occur in  $f_r(\theta_v)$  as  $\theta_i$  increases, specifically that  $f_r(\theta_v)$  tends to increase in the specular direction. Therefore, the BRDF of a sample must be determined at the angles for which it will be used for calibrations, and not inferred from

measurements with different geometries, particularly from directional-hemispherical measurements. Figure 7 also shows that reciprocity,  $f_r(\theta_i, \theta_v) = f_r(\theta_v, \theta_i)$ , holds for each sample. For example, for Spectralon,  $f_r(0^\circ, 45^\circ) = f_r(45^\circ, 0^\circ) = 0.325$ .

### *B. NIST Results*

The BRDFs measured by NIST are used as the basis for comparisons with the other participating laboratories. This is reasonable since NIST was the central laboratory of the round-robin, and therefore measured the samples on multiple occasions, and maintains the United States standards for reflectance. Indeed, both SBRS and UA use relative techniques for measuring BRDF that are based on reflectance standards supplied by NIST.

The samples were measured at NIST on the dates shown in Table 2. All the viewing angles specified by the protocol were measured on the first and last dates, while the viewing angles increment was  $20^\circ$  on the other dates. To compare the BRDFs measured on all dates, for each date, sample,  $\theta_i$ , and  $\lambda$ ,  $f_r(\theta_v)$  is fit with a natural cubic spline for  $\theta_v = -60^\circ$  to  $+60^\circ$  every  $10^\circ$ , skipping  $\theta_v = -\theta_i$ . The resulting BRDFs for each sample,  $\theta_i$ ,  $\theta_v$ , and  $\lambda$  are averaged for all dates, and the differences from the average for each date are calculated.

Plots of this difference as a function of viewing angle are used to determine the repeatability of the measurements, as well as to identify instances in which there was a problem with the measurement, particularly when the samples were obviously misaligned. Instead of showing all these plots, selected examples are shown that illustrate the best repeatability and most obvious measurement problems obtained for each sample, Figs. 8 and 9, respectively. For both figures, the difference relative to the

average,  $\Delta f_r$ , is plotted as a function of viewing angle, and the wavelength and incident angle for which these are plotted are indicated in each panel.

From Fig. 8, there is no consistent trend in  $\Delta f_r$  with date. Rather,  $\Delta f_r$  for the different dates is distributed randomly about the average. The best repeatability was obtained for Spectralon and pressed PTFE, with sintered PTFE and then aluminum having successively poorer repeatability. As shown in Fig. 7, the BRDF has a strong dependence on both incident and viewing angle, with this dependence increasing with incident angle. Therefore, a misalignment of a sample on a particular date, so that the angles of incidence and viewing are offset from their nominal values, will result in  $\Delta f_r(\theta_v)$  depending on both  $\partial f_r / \partial \theta_i$  and  $\partial f_r / \partial \theta_v$ . The clearest example of this is shown in Figs. 9(c) and 9(d) for the measurements in July 1997 and March 1997, respectively. Since  $\partial f_r / \partial \theta_i$  changes sign at approximately  $\theta_i = -30^\circ$  for both of these samples, as does  $\Delta f_r$ , this implies that the primary contribution to  $\Delta f_r$  comes from misalignment of  $\theta_i$ . From Fig. 9(b), the measurements in November 1997 were clearly wrong for pressed PTFE, but there is no correlation of  $\Delta f_r$  with  $\theta_i$  or  $\theta_v$  as there is for sintered PTFE and aluminum.

Since the results demonstrate that the reflecting properties of the samples did not change over the course of the round-robin, the BRDFs for all the dates are averaged to obtain the final values for the NIST measurements, excluding those dates on which there was an obvious problem such as misalignment. The dates and wavelengths that were excluded from the average are given in Table 3. The standard uncertainty in the average BRDF due to random effects, either from the samples or the instrument, is the standard deviation of the BRDFs, which is generally less than 0.5 %.

### *C. Participant Results*

The specific measurements made by the participants are given in Table 4. Note that none of the participants exactly followed the measurement protocol for the round-robin. SBRS did not measure the aluminum sample, and only GSFC measured at the wavelengths given by the protocol; the wavelengths used by the other participants were limited by the instrumentation, specifically laser lines for JPL and interference filters for UA. All the participants measured at all the incident angles, while only GSFC and JPL measured at all the viewing angles. Instrument design limited the SBRS viewing angles to less than the incident angle and determined the UA viewing angles that were skipped. Fortunately, as detailed below, these deviations from the protocol did not compromise the usefulness of the results obtained from this round-robin.

The primary purpose of this round-robin is to compare the BRDFs measured by the participants with the BRDF measured by NIST. Therefore, the difference in BRDF  $\Delta f_r$  between the participants and NIST is calculated for each possible sample, incident and viewing angle, and wavelength. As shown in Table 4, this calculation is not possible for each sample or viewing angle. However, for wavelength, the differences are calculated using the participant values measured closest in wavelength to the protocol wavelengths. This wavelength pairing is given in Table 5, and is reasonable since the BRDFs of all the samples are weakly dependent on wavelength.

The relative differences in BRDF between the participants' values and the NIST values as a function of viewing angle,  $\Delta f_r(\theta_v)$  are shown in Figs. 10 to 21. Each figure is for a given sample and wavelength, with the panels showing the results for all the participants at different incident angles. Differences for wavelengths of only 440 nm,

633 nm, and 860 nm are given since the other wavelengths both were not used by all the participants and yielded similar differences to the ones shown in the figures. The results presented in these figures are somewhat overwhelming because of the number of parameters involved – sample, wavelength, incident angle, participant, and viewing angle. Therefore, the discussion in the next two paragraphs concentrates on the dependencies of the differences on viewing angle, first by sample and then by participant, while more specific conclusions from these results are presented in succeeding paragraphs.

In nearly all cases,  $\Delta f_r(\theta_v)$  is greater than the standard deviation of the NIST values for BRDF. For Spectralon,  $\Delta f_r$  generally does not depend on  $\theta_v$ , except for a slight dependence for GSFC at all wavelengths and at larger  $\theta_i$  and  $\theta_v$ , and for JPL at  $\lambda = 860$  nm. With pressed PTFE, GSFC has the same dependence as with Spectralon, while there are possible sample misalignments for JPL at  $\lambda = 440$  nm and 633 nm and for SBRS at  $\lambda = 440$  nm and  $\theta_i = 60^\circ$ . Accurate measurements on the sintered PTFE sample were difficult because of the wedge of the surface relative to the holder, and this is seen in  $\Delta f_r(\theta_v)$ . The misalignment is apparent for UA and somewhat for GSFC at all wavelengths, and probably for JPL at  $\lambda = 440$  nm and 860 nm. Surprisingly,  $\Delta f_r$  for SBRS does not depend on  $\theta_v$ , indicating that the sample alignment procedure for this participant accounted for the wedge resulting in no misalignment of  $\theta_i$ . Finally, all participants have large values of  $\Delta f_r$  for aluminum at  $\theta_i = 0^\circ$ ,  $\theta_v = \pm 10^\circ$ ; even the NIST values have a standard deviation of 3 %. This is probably because  $f_r$  for aluminum is sharply peaked at  $\theta_i = \theta_v = 0^\circ$ , as seen in Fig. 5(b), and is therefore more sensitive to

misalignments at these angles than are the other samples. For all the participants,  $\Delta f_r$  of aluminum does not depend on  $\theta_v$ .

In several cases,  $\Delta f_r$  for GSFC has a slight dependence on  $\theta_v$ , especially for large  $\theta_i$  and  $\theta_v$ . In contrast, there is no such general dependence with the other participants; a dependence of  $\Delta f_r$  on  $\theta_v$  usually indicates a misalignment of the sample. This is especially apparent for UA with the wedged sintered PTFE sample.

To make further progress in analyzing the participant BRDFs for dependencies on sample, wavelength, incident angle, and participant, the results shown in Figs. 10 to 21 must be simplified so that they are tractable. This is done by averaging  $\Delta f_r$  over  $\theta_v$ , which is reasonable since the dependence on  $\theta_v$  is usually slight. This procedure yields a concise method for determining systematic differences between a participant's BRDF values and those of NIST, and for assessing the uncertainties, although the information about  $\Delta f_r(\theta_v)$  is lost. The average relative difference in BRDF,  $\langle \Delta f_r \rangle$ , between the participants' values and the NIST values as a function of wavelength are shown in Figs. 22 to 25, and include those wavelengths not shown in Figs. 10 to 21. Each figure is for a given participant, with the panels showing the results for each sample. The horizontal dashed lines are the expanded uncertainties ( $k = 2$ ) for each sample and participant, as detailed in the next paragraph.

The components of uncertainty in the NIST values of BRDF are those arising both from random effects – source stability, signal noise, and sample repeatability – and from systematic effects – incident angle, aperture area, and distance from aperture to sample. The standard uncertainties from the random effects for each sample, wavelength, and incident angle were evaluated using a Type A method (Taylor 1994) as the average

standard deviation for all viewing angles at a wavelength of 440 nm. Only this wavelength is used since the average standard deviations at other wavelengths are nearly identical to those at  $\lambda = 440$  nm. The standard uncertainties for the systematic effects are evaluated using a Type B method (Taylor 1994) and are detailed in (Barnes 1998a). The standard uncertainties from these evaluations are given in Table 6. The standard uncertainties in the participants' values of BRDF are either in the literature or were communicated to NIST, and are given in Table 7. The ultimate goal of the uncertainty analysis is to obtain a single uncertainty for the average relative difference of BRDF for each sample and participant, independent of incident angle. Therefore, the maximum Type A and B standard uncertainties from NIST for each sample, and the participant's standard uncertainty, are used to calculate the combined standard uncertainty of the average relative difference. The resulting expanded uncertainties ( $k = 2$ ) for each sample and participant are given in Table 8.

The average relative difference of BRDF for GSFC, shown in Fig. 22, has a slight dependence on wavelength, generally decreasing as the wavelength increases. There is also a similar dependence on incident angle, though this could be a result of the dependence on the viewing angle discussed above. As expected from the BRDF properties of the samples,  $\langle \Delta f_r \rangle$  for the aluminum sample has a greater range than it does for the other samples. In nearly all cases,  $\langle \Delta f_r \rangle$  is less than the expanded uncertainties for each sample. Finally,  $\langle \Delta f_r \rangle$  for the Spectralon and pressed PTFE samples averages 0.25 % to 0.5 % over wavelength, suggesting that the GSFC values for BRDF are systematically higher than those obtained by NIST by this amount. For JPL, shown in Fig. 23,  $\langle \Delta f_r \rangle$  at  $\lambda = 440$  nm is systematically greater than it is at the other wavelengths

for all the samples, while at  $\lambda = 633$  nm and 860 nm  $\langle \Delta f_r \rangle$  averages  $-0.5$  % to  $-1.0$  %. Also, the dependence of  $\langle \Delta f_r \rangle$  on wavelength is similar for all samples. Because of the relatively large uncertainty in absolute BRDF for JPL, as compared to the other participants,  $\langle \Delta f_r \rangle$  is always less than the expanded uncertainty. The systematic difference at  $\lambda = 440$  nm is not expected to be a problem for the normalized BRDF measurements for MISR since the normalization is between angles, not wavelengths, and the differences at each wavelength are nearly the same for all angles. This is illustrated at the end of this section.

The average relative difference of BRDF for SBRS, shown in Fig. 24, has no systematic dependence on either wavelength or incident angle, even for the sintered PTFE sample, and is less than the expanded uncertainty except at  $\lambda = 440$  nm for pressed PTFE. The average  $\langle \Delta f_r \rangle$  is  $-0.5$  %. Similar results for the wavelength dependence were obtained for UA, shown in Fig. 25. However,  $\langle \Delta f_r \rangle$  depends significantly on the incident angle for the sintered PTFE sample, illustrating again the difficulties encountered with measuring this sample because of the wedge of the surface relative to the holder. Even so, because of the relatively large standard uncertainty assigned by the participant,  $\langle \Delta f_r \rangle$  is less than the expanded uncertainties except for the aluminum sample at  $\theta_i = 0^\circ$ . This exception indicates that there was a problem with this particular measurement since  $\langle \Delta f_r \rangle$  for the other incident angles are similar to those for the Spectralon and pressed PTFE samples. The average  $\langle \Delta f_r \rangle$  for the Spectralon and pressed PTFE samples is  $-0.75$  %, which is similar to the results obtained for JPL and SBRS, indicating that the assigned standard uncertainty for UA is probably too large.

Since MISR uses a detector standard at a fixed  $\theta_v = 10^\circ$  to monitor the reflectance of the on-board Spectralon diffuser (Diner 1998), the quantity of interest for this instrument is the normalized BRDF – the BRDF for a given set of parameters divided by the BRDF with one of the parameters held fixed. This quantity is also called the relative BRDF, but the term normalized will be used to avoid confusing terminology in this paper. Therefore, for the sake of completeness, it is useful to analyze the results of the round-robin for the Spectralon sample in terms of normalized BRDF.

For the Spectralon sample, the BRDF values measured by NIST and each participant for each wavelength and incident angle were normalized by the BRDF at  $\theta_v = 10^\circ$ . The relative differences in normalized BRDF between the participants' values and the NIST values as a function of viewing angle are shown in Figs. 26 to 28, which are analogous to Figs. 10 to 12. As expected from the normalization, for those participants in Figs. 10 to 12 for which  $\Delta f_r$  does not depend strongly on  $\theta_v$ , even though  $\Delta f_r$  may be large,  $\Delta f_r$  in Figs. 26 to 28 is small. This is particularly apparent for the measurements made by JPL. On the other hand, if  $\Delta f_r$  in Figs. 10 to 12 does depend on  $\theta_v$ , which is usually the case for GSFC, then  $\Delta f_r$  in Figs. 26 to 28 has the same dependence.

Finally, the analogue of Figs. 22 to 25 for normalized BRDF is shown in Fig. 29, where the average relative difference in normalized BRDF between the participants' values and the NIST values,  $\langle \Delta f_r \rangle$ , is plotted as a function of wavelength. The horizontal dashed lines are the expanded uncertainties ( $k = 2$ ) for each participant, and were calculated using the components of uncertainty in the NIST values arising from random effects (from Table 6) and the standard uncertainties in the participants' values (from Table 7). For all participants,  $\langle \Delta f_r \rangle$  does not depend on wavelength or incident angle,

and is less than the expanded uncertainties. In fact, for GSFC,  $\langle \Delta f_r \rangle$  is less than 0.75 %, whereas for the other participants  $\langle \Delta f_r \rangle$  is less than 0.5 %.

In general, the average difference in BRDF is less than the expanded uncertainty for all the participants and samples, except for UA for sintered PTFE and aluminum. None the less, there are systematic differences of 0.5 % to 1 % between the participant's BRDF values and those of NIST, while the largest differences are usually less than 2 % when the exceptions noted above are disregarded. There is no obvious correlation between the differences and the method a laboratory uses to measure BRDF – either absolute or relative to NIST standards. Therefore, the overall expanded uncertainty ( $k = 2$ ) of BRDF measurements of diffuse reflectors in the EOS program should be considered to be 2 %. Those interested in a particular participating laboratory, sample, wavelength, and bidirectional angle combination should consult the results for that situation, specifically Figs. 10 to 21. Note that in some of these cases the difference in BRDF between NIST and a participant can be larger than the expanded uncertainty, sometimes much larger.

#### **IV. Conclusions**

The round-robin measurements of BRDF among laboratories participating in EOS programs were completed successfully. The BRDF of all the samples – Spectralon, pressed and sintered PTFE, and aluminum – is spectrally neutral for wavelengths from 440 nm to 940 nm and depends on both the incident and viewing angles. For all incident angles, the BRDF as a function of viewing angle tends to increase in the specular direction. The BRDF of the samples was repeatable, although more so for the Spectralon

and pressed PTFE samples than for sintered PTFE and aluminum, with no trends with time. This repeatability, together with the spectral neutrality, aided comparison of the BRDF values between the participants and NIST since the experimental protocol was not always followed.

Differences in BRDF values depend on the participant, sample, incident and viewing angles, and wavelength. Analysis of these differences was simplified by averaging over the viewing angles. There were few obvious problems with the measurements. Two participants had difficulty measuring the sintered PTFE sample because of a tilt in the surface, and the BRDF values of JPL at a wavelength of 440 nm are always larger than both those measured at other wavelengths and those measured by NIST and the other participants. All participants have systematic differences between their BRDF values and those measured by NIST, generally less than 1.5 %, and these differences are in most cases less than the expanded uncertainty. Therefore, this round-robin has shown, with the exception of the problems detailed above, that all the participating laboratories are capable of performing BRDF measurements on a variety of samples at various wavelengths and angles that differ from the NIST values by generally less than 2 %. This is considered to be good agreement and indicates the overall uncertainty of BRDF measurements of diffuse reflectors in the EOS program.

### **Acknowledgements**

The JPL measurements were performed by David A. Haner at the Department of Chemistry, California State Polytechnic University, Pomona, California, and analyzed by Nadine L. Chrien at JPL. Guojun Si at Swales Aerospace, Beltsville, Maryland,

measured the samples and reduced the data for GSFC. The work at UA was supported by NASA contract NAS5-31717 and at NIST by the NASA EOS Project Science Office (S-41365-F).

## References

- ASTM 1997: "E1392-90, Standard Practice for Angle Resolved Optical Scatter Measurements on Specular or Diffuse Surfaces," in *Annual Book of ASTM Standards, Vol. 10.05: Electrical Insulation and Electronics*, American Society for Testing and Materials, West Conshohocken, PA.
- Barnes, P. Y., Early, E. A., and Parr, A. C., 1998a: "Spectral Reflectance," *NIST Special Publication 250-48*, U. S. Department of Commerce, National Institute of Standards and Technology, Gaithersburg, MD.
- Barnes, P. Y., Early, E. A., Johnson, B. C., Butler, J. J., Bruegge, C. J., Biggar, S., Spyak, P. R., and Pavlov, M., 1998b: "Intercomparisons of Reflectance Measurements," *Proc. SPIE 3425*, 10.
- Biggar, S. F., Labed, J., Santer, R. P., Slater, P. N., Jackson, R. D., and Moran, M. S., 1988: "Laboratory Calibration of Field Reflectance Panels," *Proc. SPIE 924*, 232.
- Butler, J. J. and Johnson, B. C., 1996a: *The Earth Observer* 8(1), 22.
- Butler, J. J. and Johnson, B. C., 1996b: *The Earth Observer* 8(2), 26.
- Clarke, F. J. J., Garforth, F. A., and Parry, D. J., 1983: "Goniophotometric and Polarization Properties of White Reflection Standard Materials," *Lighting Res. Tech.* 15, 133.

- Diner, D. J., Bechert, J. C., Reilly, T. H., Bruegge, C. J., Conel, J. E., Kahn, R. A., Martonchik, J. V., Ackerman, T. P., Davies, R., Gerstl, S. A., Gordon, H. R., Muller, J. P., Myneni, R., Sellers, P. J., Pinty, B., and Verstraete, M. M., 1998: "Multi-Angle Imaging Spectroradiometer (MISR) Instrument Description and Experiment Overview," *IEEE Trans. Geosci. Remote Sensing* **36**, 1072.
- Guenther, B., Barnes, W., Knight, E., Barker, J., Harnden, J., Weber, R., Roberto, M., Godden, G., Montgomery, H., and Abel, P., 1996: "MODIS Calibration: A Brief Review of the Strategy for the At-Launch Calibration Approach," *J. Atmos. Oceanic Technol.* **13**, 274.
- Jaross, G., Krueger, A. L., and Wellemeyer, C., 1998: "Sensitivity of Total Ozone Mapping Spectrometer Products to Diffuse Reflectance Measurements," *Metrologia* **35**, 663.
- Johnson, B. C., Barnes, P. Y., O'Brian, T. R., Butler, J. J., Bruegge, C. J., Biggar, S., Spyak, P. R., and Pavlov, M. M., 1998: "Initial Results of the Bidirectional Reflectance Characterization Round-Robin in Support of EOS," *Metrolgia* **35**, 609.
- Leonard, T. A. and Pantoliano, M., 1988: "BRDF Round Robin," *Proc. SPIE* **967**, 226.
- McGuckin, B. T., Haner, D. A., Menzies, R. T., Esproles, C., and Brothers, A. M., 1996: "Directional Reflectance Characterization Facility and Measurement Methodology," *Appl. Optics* **35**, 4827.
- Nicodemus, F. E., Richmond, J. C., Hsia, J. J., Ginsberg, I. W., and Limperis, T., 1977: "Geometrical Considerations and Nomenclature for Reflectance," *NBS Monograph 160*, U.S. Department of Commerce, National Bureau of Standards, Gaithersburg, MD.

- Park, H., Krueger, A., Hilsenrath, E., Jaross, G., and Haring, R., 1996: "Radiometric Calibration of Second Generation Total Ozone Mapping Spectrometer (TOMS)", *Proc. Intl. Soc. Opt. Engr.* **2820**, 162.
- Proctor, J. E. and Barnes, P. Y., 1996: "NIST High Accuracy Reference Reflectometer-Spectrophotometer," *J. Res. Natl. Inst. Stand. Technol.* **101**, 619.
- Schiff, T. F., Knighton, M. W., Wilson, D. J., Cady, F. M., Stover, J. C., and Butler, J. J., 1993: "Design Review of a High Accuracy UV to Near IR Scatterometer," *Proc. SPIE* **1995**, 12.
- Spyak, P. R. and Lansard, C., 1997: "Reflectance Properties of Pressed Algoflon F6: A Replacement Reflectance-Standard Material for Halon," *Appl. Opt.* **36**, 2963.
- Slater, P. N., Biggar, S. F., Thome, K. J., Gelman, D. I., and Spyak, P. R., 1996: "Vicarious Radiometric Calibrations of EOS Sensors," *J. Atmos. Oceanic Technol.* **13**, 349.
- Taylor, B. N. and Kuyatt, C. E., 1994: "Guidelines for Evaluating and Expressing the Uncertainty of NIST Measurement Results," *NIST Technical Note 1297*, U. S. Department of Commerce, National Institute of Standards and Technology, Gaithersburg, MD.
- Weidner, V. R. and Hsia, J. J., 1981: "Reflection Properties of Pressed Polytetrafluoroethylene Powder," *J. Opt. Soc. Am.* **71**, 856.
- Wells, C., Pellicori, S. F., and Pavlov, M., 1994: "Polarimetry and Scatterometry Using a Wollaston Polarimeter," *Proc. SPIE* **2265**, 105.

## Tables

Table 1. Experimental protocol parameters for the EOS BRDF round-robin comparison

Parameter	Value
Samples	Spectralon, pressed PTFE, sintered PTFE, aluminum
Wavelengths [nm]	440, 550, 633, 670, 860, 940, 1240
Bandwidth [nm]	10
Incident polar angles [deg]	0, 30, 45, 60
Viewing polar angles [deg]	-60 to 60 in steps of 10
Measurement plane	In-plane
Polarization state	Report BRDF for unpolarized light
Sample size	50.8 mm diameter
Sample alignment	Fiducial mark on holder

Table 2. Dates on which participating laboratories measured the round-robin samples

Participant	Date
NIST	October 1996
JPL	November 1996
NIST	February 1997
UA	February 1997
NIST	March 1997
SBRS	April 1997
NIST	July 1997
GSFC	August 1997
NIST	November 1997

Table 3. Dates and wavelengths excluded from the average BRDF of the NIST values for each sample.

Sample	Date	Wavelength Range [nm]
Spectralon	February 1997	440 to 940
Spectralon	July 1997	440 to 940
pressed PTFE	November 1997	440 to 670
sintered PTFE	July 1997	440 to 940
sintered PTFE	November 1997	440 to 670
Aluminum	March 1997	440 to 670

Table 4. Measurement parameters of the participating laboratories

Parameters	Participating Laboratory			
	GSFC	JPL	SBRS	UA
Samples*	A, B, C, D	A, B, C, D	A, B, C	A, B, C, D
Wavelengths [nm]	440, 550, 633, 670, 860	442, 632, 860	400, 500, 600, 700, 900, 1700	455, 554, 647, 860, 949
Incident Angles	0°, 30°, 45°, 60°	0°, 30°, 45°, 60°	0°, 30°, 45°, 60°	0°, 30°, 45°, 60°
Viewing Angles				
Range	-60° to 60°	-85° to 85°	<u><math>\theta_i</math></u> range 0° -60° to -10° 30° -50° to 20° 45° -65° to 35° 60° -60° to 50°	-60° to 60°
Increment	10°	5°	10°	10°
	skip $\theta_v = \theta_i$	skip $\theta_v = \theta_i$		<u><math>\theta_i</math></u> skip 0° 0°, 10° 30° 30° 45° 50° 60° 60°

\* Sample A – Spectralon, B – pressed PTFE, C – sintered PTFE, D – aluminum

Table 5. Wavelengths at which BRDF was measured for each participating laboratory used to calculate the difference with the BRDF values measured at the NIST wavelengths

NIST	GSFC	JPL	SBRS	UA
Wavelength [nm]				
440	440	442	400	455
550	550		500	554
633	633	633	600	647
670	670		700	
860	860	860	900	860
940			900	949

Table 6. Standard uncertainties of the NIST values of BRDF

	Standard Uncertainty [%]			
	Incident Angle [deg]			
	0	30	45	60
Type A Evaluation				
Spectralon	0.21	0.15	0.24	0.22
pressed PTFE	0.20	0.21	0.20	0.28
sintered PTFE	0.47	0.34	0.44	0.58
Aluminum	0.82	0.49	0.58	0.66
Type B Evaluation	0.06	0.10	0.15	0.25

Table 7. Standard uncertainties of the participant values of BRDF

Participant	Standard Uncertainty [%]
GSFC	0.6
JPL	5.0 (absolute) 0.2 (relative)
SBRS	0.6
UA	2.0

Table 8. Maximum expanded uncertainty ( $k = 2$ ) of the combined standard uncertainties from NIST and each participant

Sample	Expanded Uncertainty ( $k = 2$ ) [%]			
	Participant			
	GSFC	JPL	SBRS	UA
Spectralon	1.4	10.0	1.4	4.1
pressed PTFE	1.4	10.0	1.4	4.1
sintered PTFE	1.7	10.1	1.7	4.2
Aluminum	2.0	10.1	2.0	4.3

## Figure Captions

- Figure 1. Schematic diagram of the angular and polarization conventions used for the BRDF measurements. Both angles are positive as shown.
- Figure 2. BRDF as a function of viewing angle for Spectralon from the NIST measurements. The incident angles are indicated in the panels, and the wavelengths are given in the legend.
- Figure 3. Same as Fig. 2 but for pressed PTFE.
- Figure 4. Same as Fig. 2 but for sintered PTFE.
- Figure 5. Same as Fig. 2 but for aluminum.
- Figure 6. BRDF as a function of wavelength from the NIST measurements. The angles are indicated in the panels, and the samples are given in the legend. The symbols for Spectralon and pressed PTFE coincide.
- Figure 7. BRDF as a function of viewing angle at a wavelength of 633 nm from the NIST measurements. The samples are indicated in the panels, the incident angles are given in the legend, and the horizontal line is the ideal value of  $1/\pi \text{ sr}^{-1}$ .
- Figure 8. Difference of BRDF relative to the average as a function of viewing angle for the best repeatability of each sample from the NIST measurements. The samples, wavelengths, and incident angles are indicated in the panels, and the measurement dates are given in the legend.
- Figure 9. Same as Fig. 8 but for the most obvious misalignment for each sample.

Figure 10. Difference of BRDF relative to the NIST value as a function of viewing angle for Spectralon at 440 nm. The incident angles are indicated in the panels, and the participants are given in the legend.

Figure 11. Same as Fig. 10 but for Spectralon at 633 nm.

Figure 12. Same as Fig. 10 but for Spectralon at 860 nm.

Figure 13. Same as Fig. 10 but for pressed PTFE at 440 nm.

Figure 14. Same as Fig. 10 but for pressed PTFE at 633 nm.

Figure 15. Same as Fig. 10 but for pressed PTFE at 860 nm.

Figure 16. Same as Fig. 10 but for sintered PTFE at 440 nm.

Figure 17. Same as Fig. 10 but for sintered PTFE at 633 nm.

Figure 18. Same as Fig. 10 but for sintered PTFE at 860 nm.

Figure 19. Same as Fig. 10 but for aluminum at 440 nm.

Figure 20. Same as Fig. 10 but for aluminum at 633 nm.

Figure 21. Same as Fig. 10 but for aluminum at 860 nm.

Figure 22. Average difference of BRDF relative to the NIST value as a function of wavelength for GSFC. The samples are indicated in the panels, and the incident angles are given in the legend. The horizontal dashed lines are the expanded uncertainty ( $k = 2$ ) of the average difference.

Figure 23. Same as Fig. 22 but for JPL. The expanded uncertainties are larger than the limits of the vertical axis.

Figure 24. Same as Fig. 22 but for SBRS.

Figure 25. Same as Fig. 22 but for UA. The expanded uncertainties in (a) and (b) are larger than the limits of the vertical axis.

Figure 26. Difference of normalized BRDF at  $\theta_v = 10^\circ$  relative to the NIST value as a function of viewing angle for Spectralon at 440 nm. The incident angles are indicated in the panels, and the participants are given in the legend.

Figure 27. Same as Fig. 26 but at 633 nm.

Figure 28. Same as Fig. 26 but at 860 nm.

Figure 29. Average difference of normalized BRDF relative to the NIST value as a function of wavelength. The participants are indicated in the panels, and the incident angles are given in the legend. The horizontal dashed lines are the expanded uncertainty ( $k = 2$ ) of the average difference. The expanded uncertainties in (d) are larger than then limits of the vertical axis.

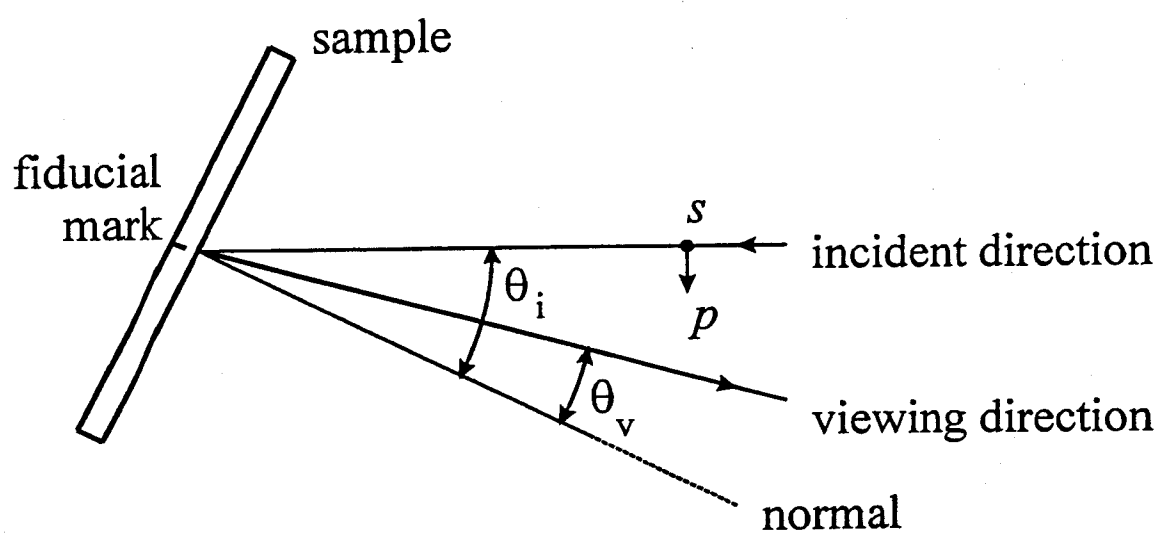


Figure 1

# Spectralon

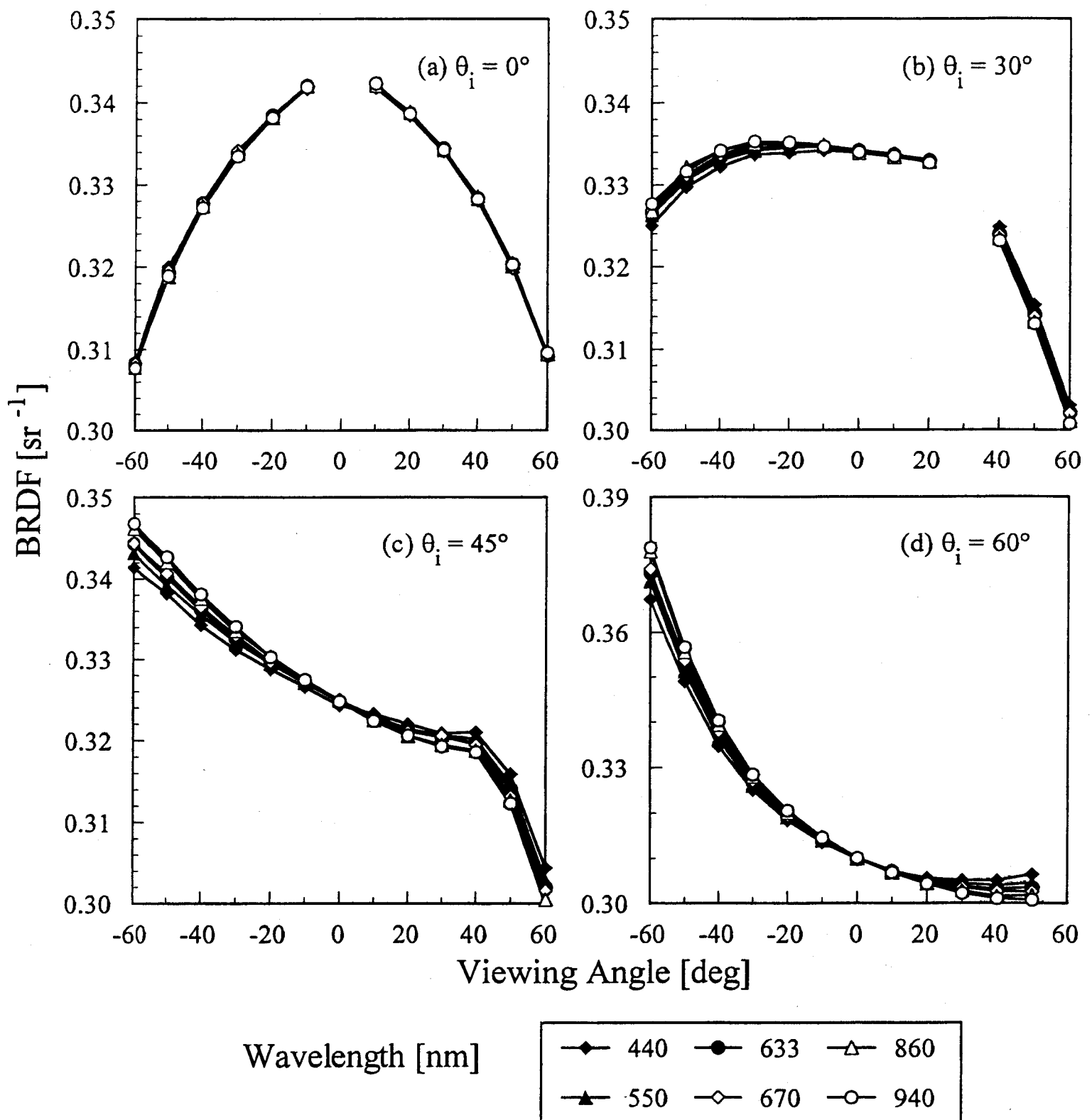


Figure 2

pressed PTFE

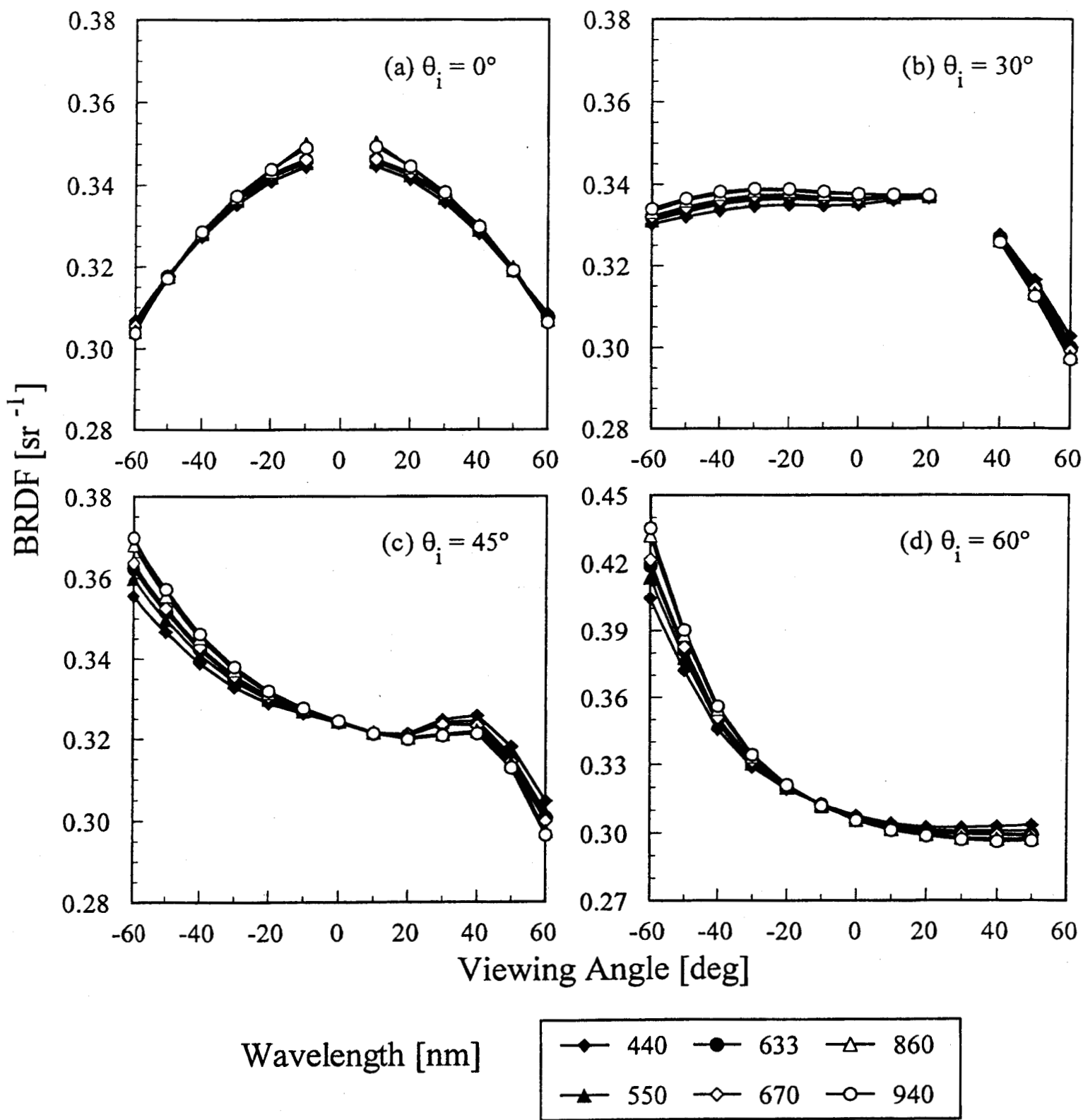


Figure 3

# sintered PTFE

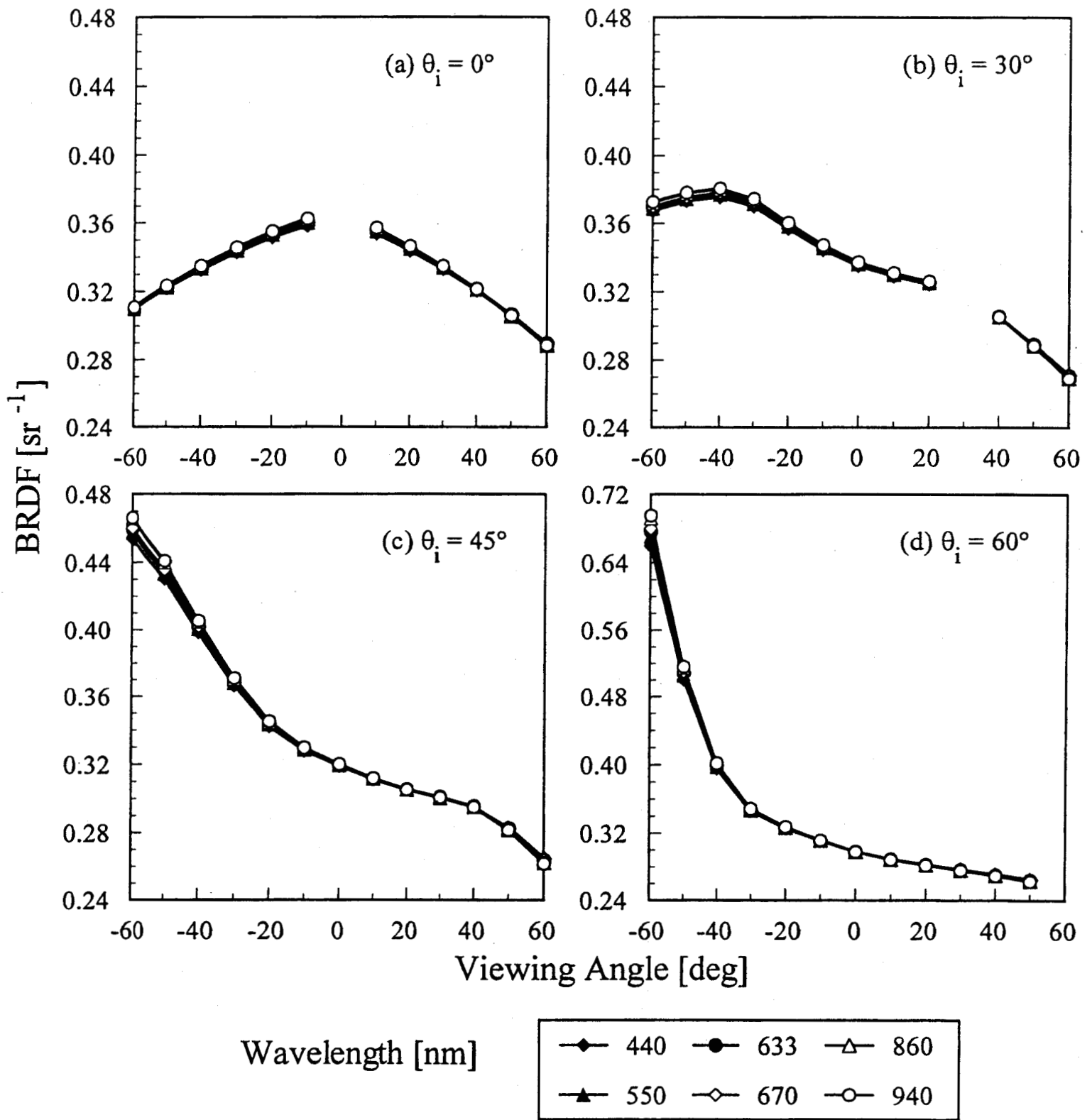


Figure 4

# Aluminum

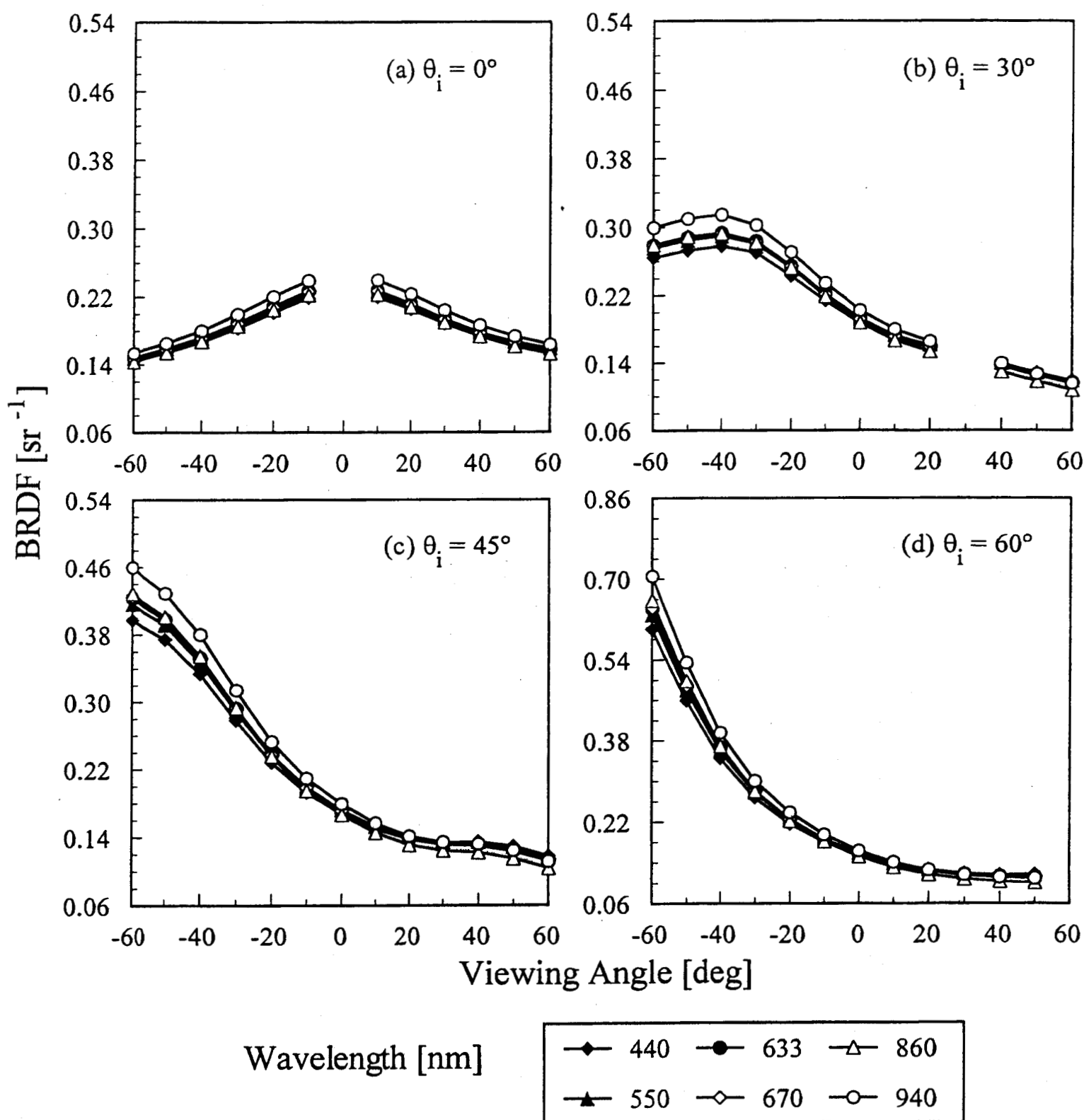


Figure 5

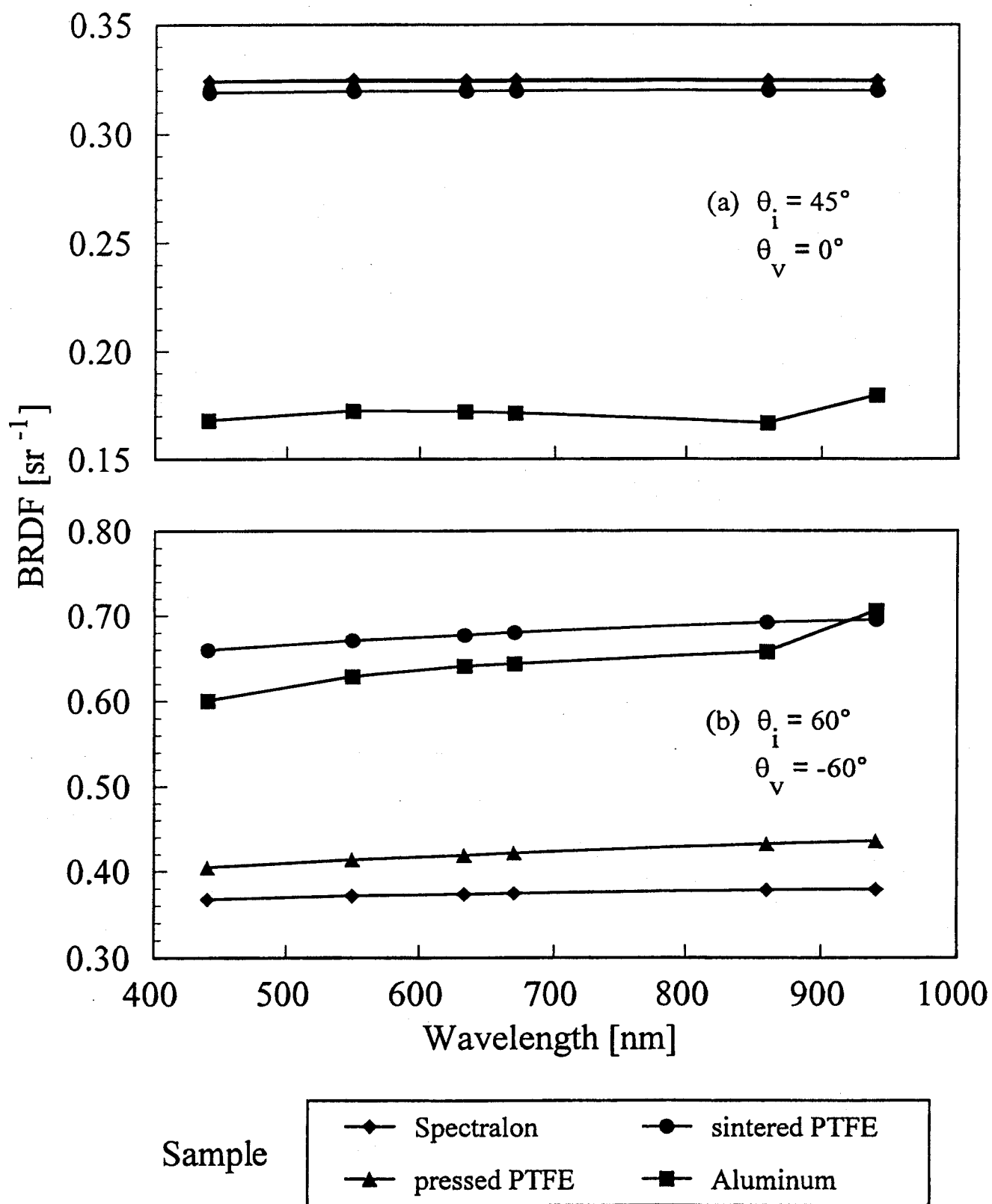


Figure 6

$\lambda = 633 \text{ nm}$

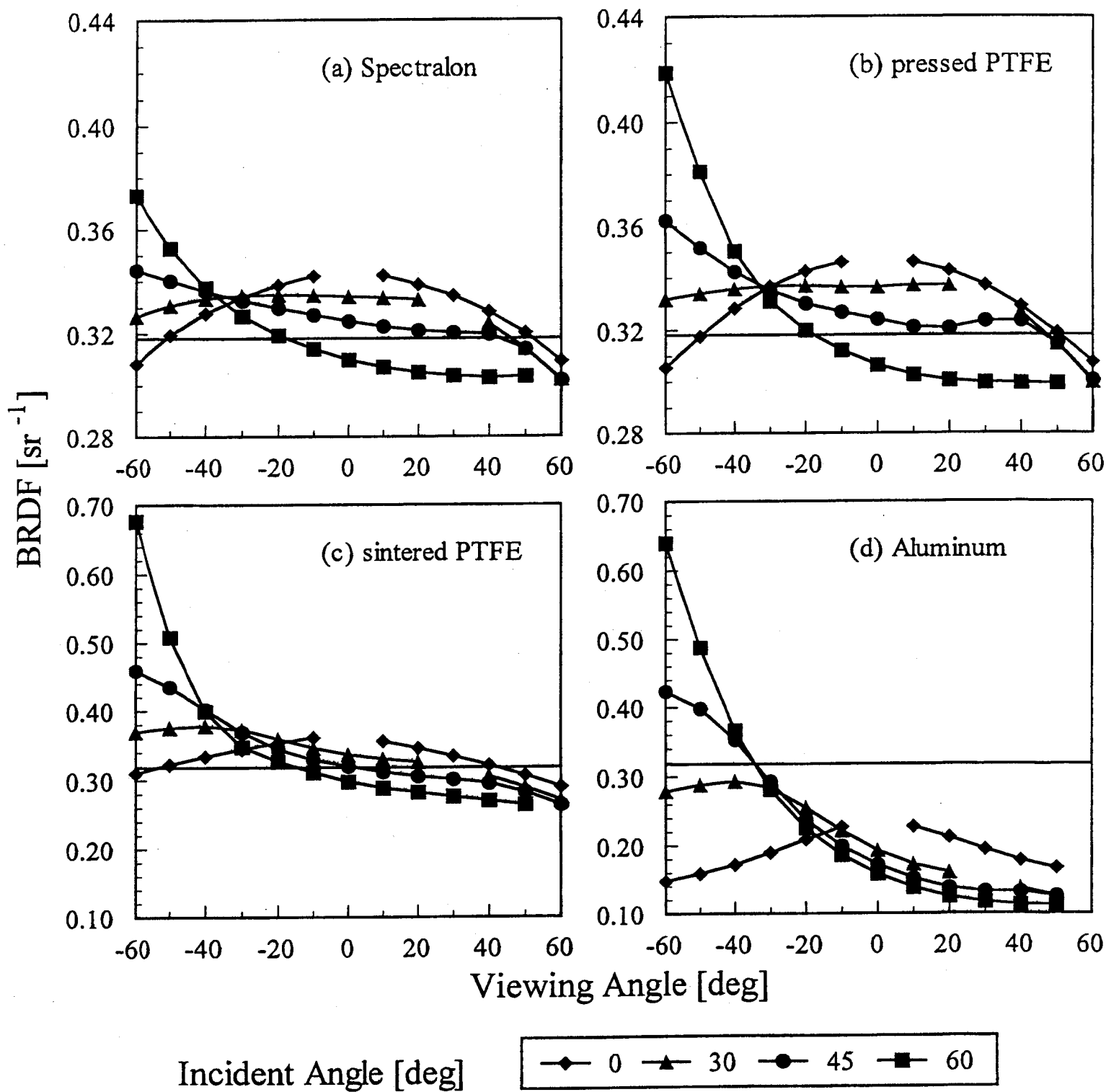
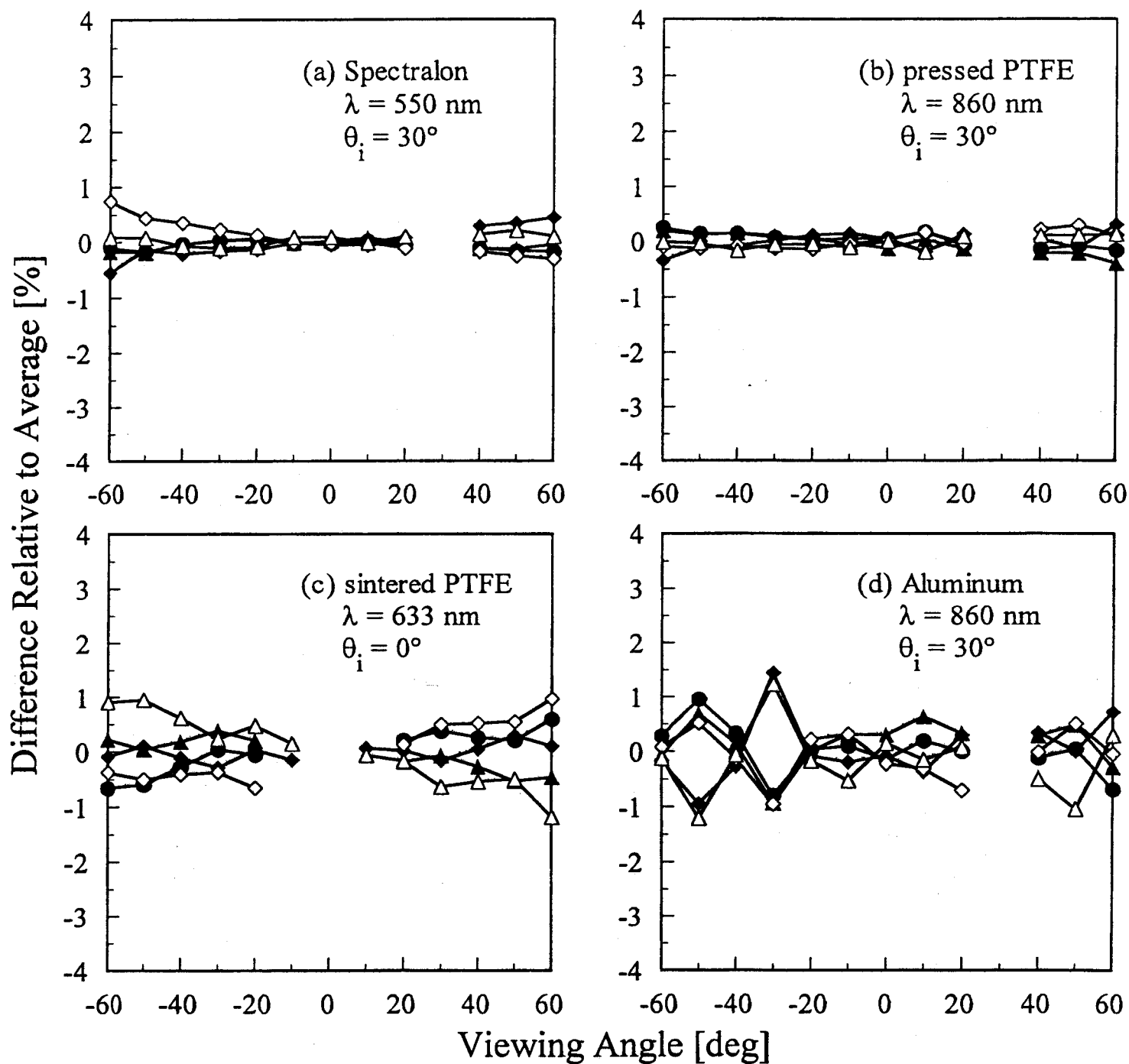


Figure 7

# Repeatability



Measurement  
Date

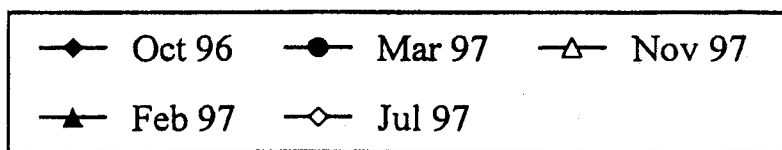


Figure 8

# Misalignment

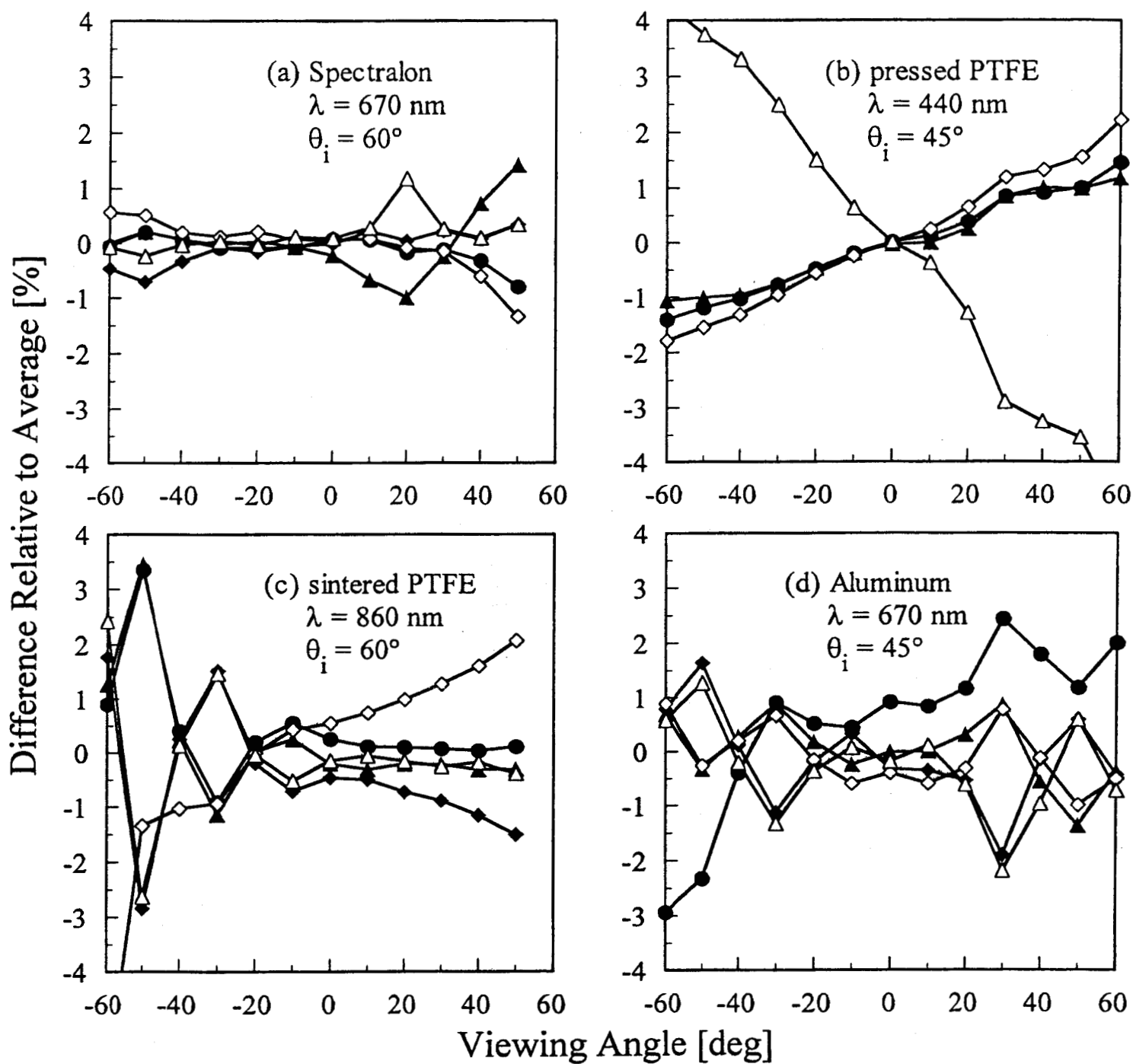


Figure 9

Spectralon,  $\lambda = 440$  nm

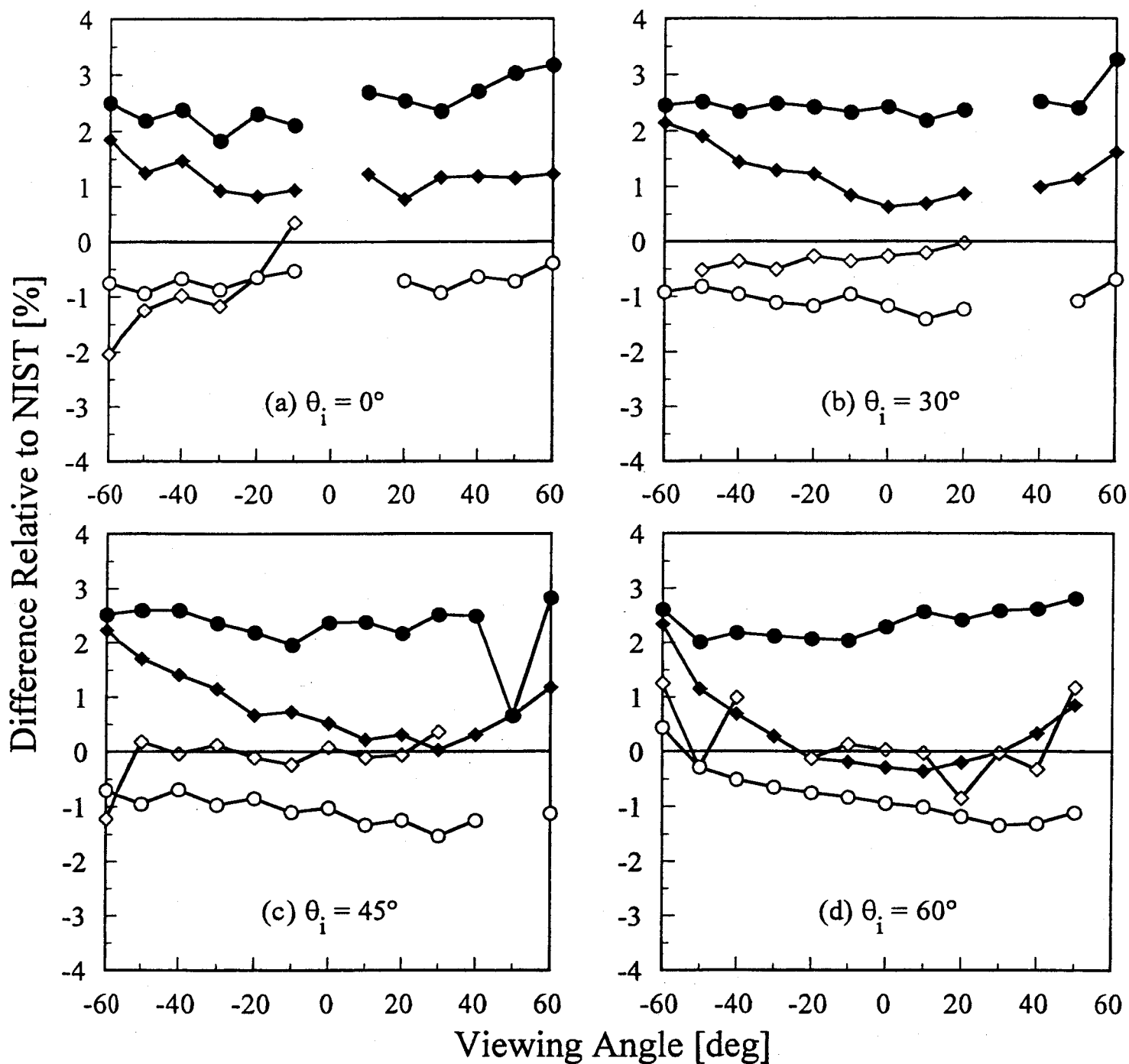


Figure 10

Spectralon,  $\lambda = 633 \text{ nm}$

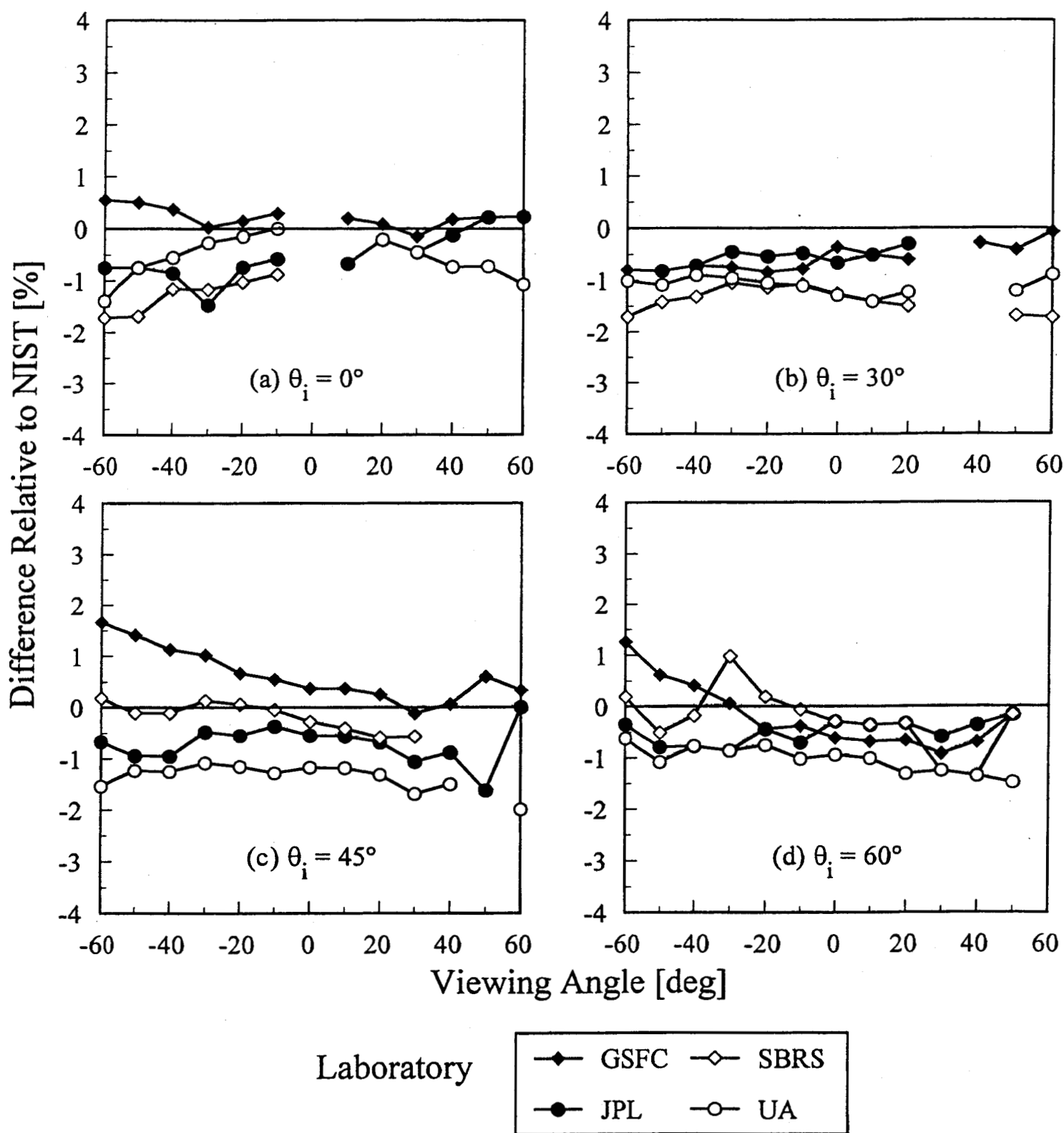


Figure 11

Spectralon,  $\lambda = 860$  nm

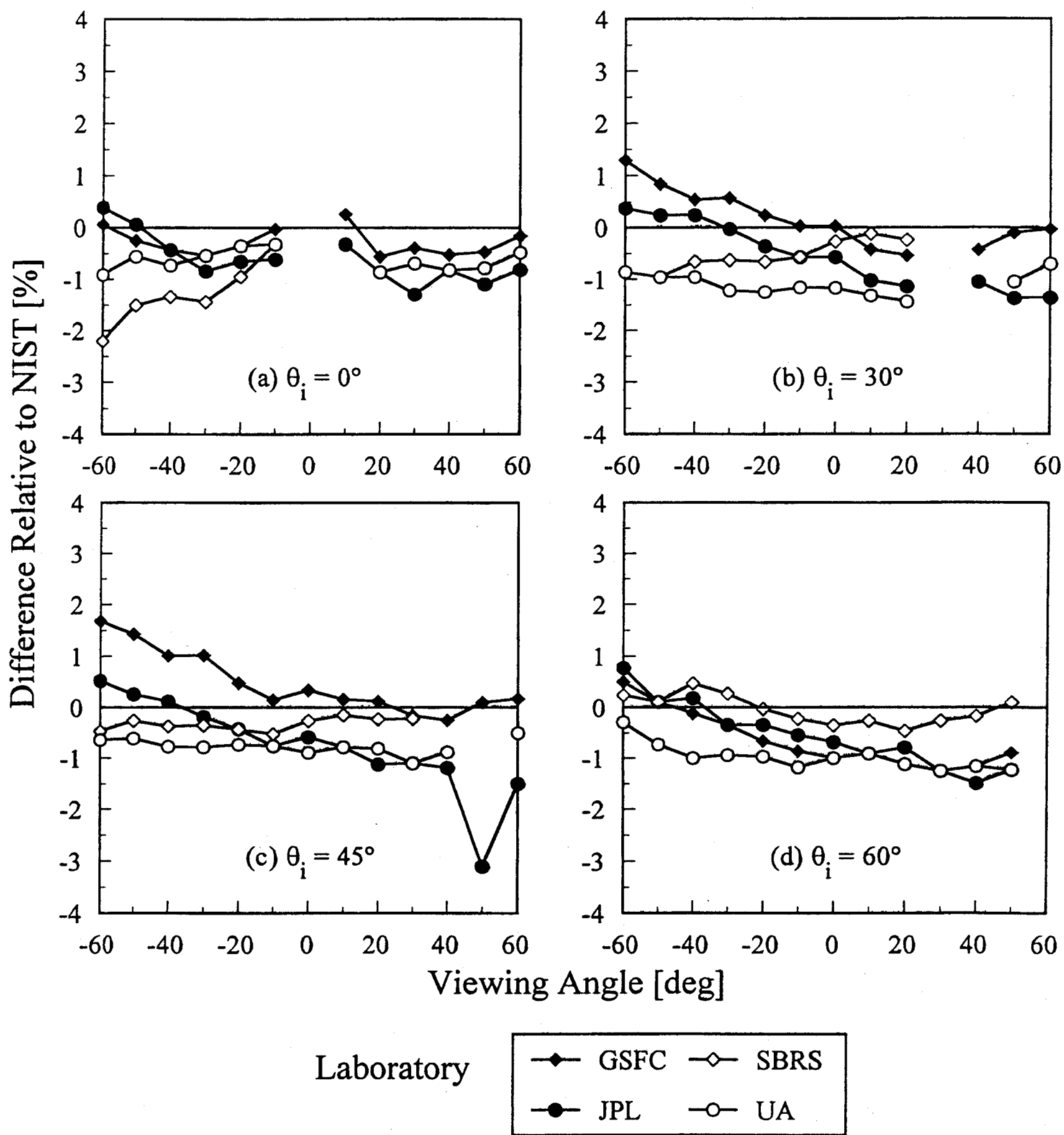
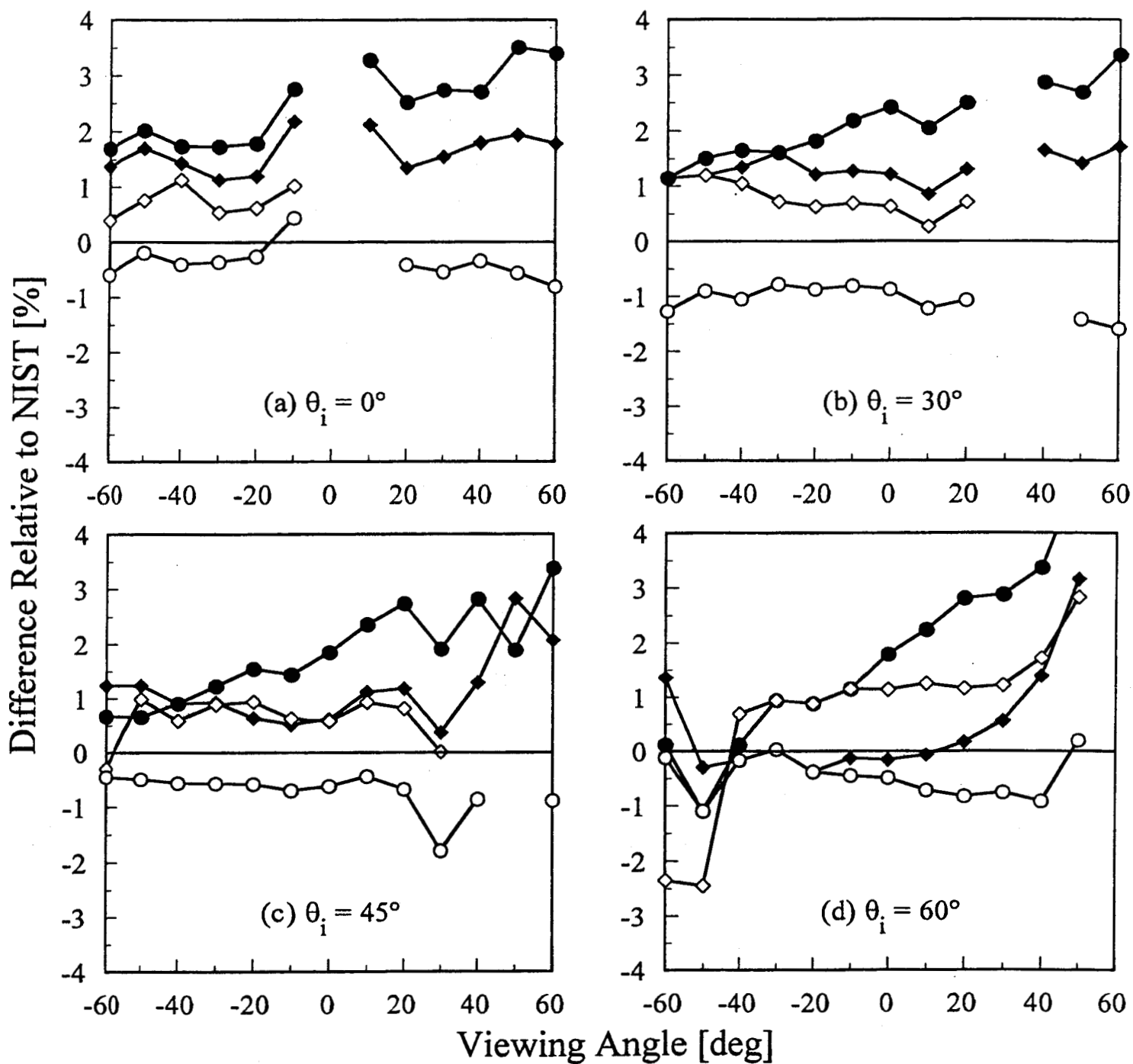


Figure 12

pressed PTFE,  $\lambda = 440$  nm



Laboratory

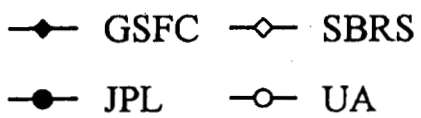


Figure 13

pressed PTFE,  $\lambda = 633$  nm

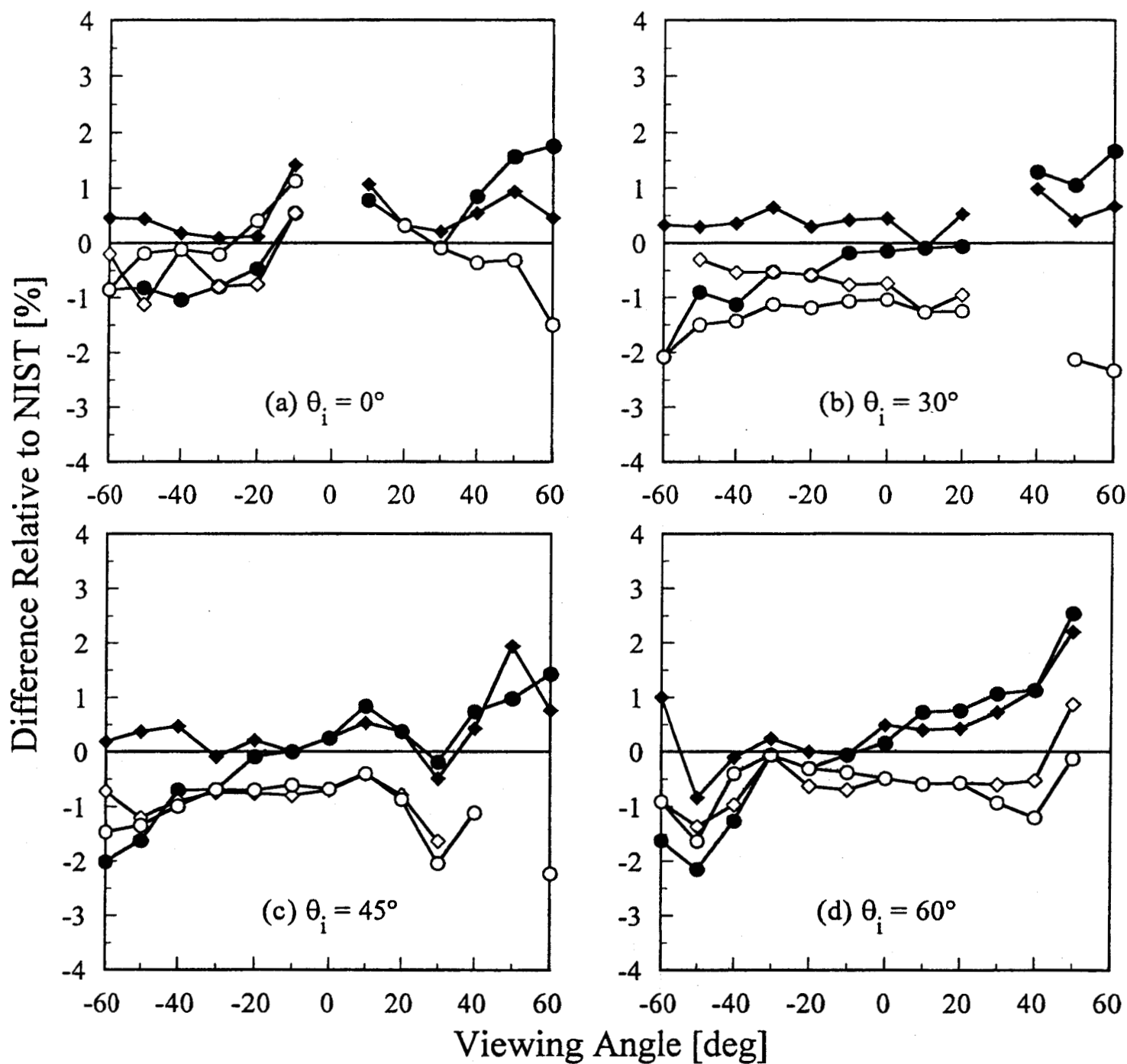


Figure 14

pressed PTFE,  $\lambda = 860$  nm

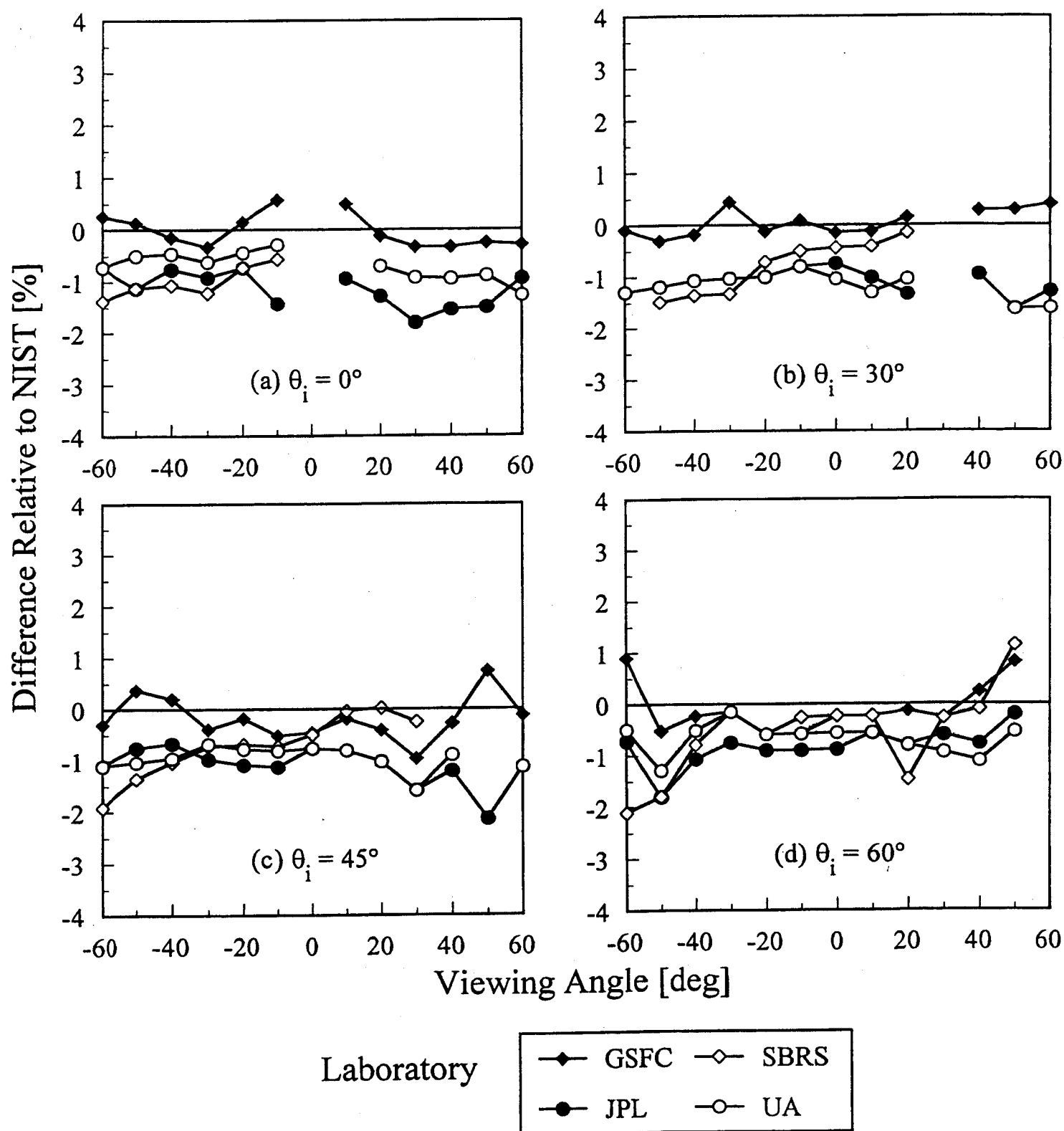


Figure 15

sintered PTFE,  $\lambda = 440$  nm

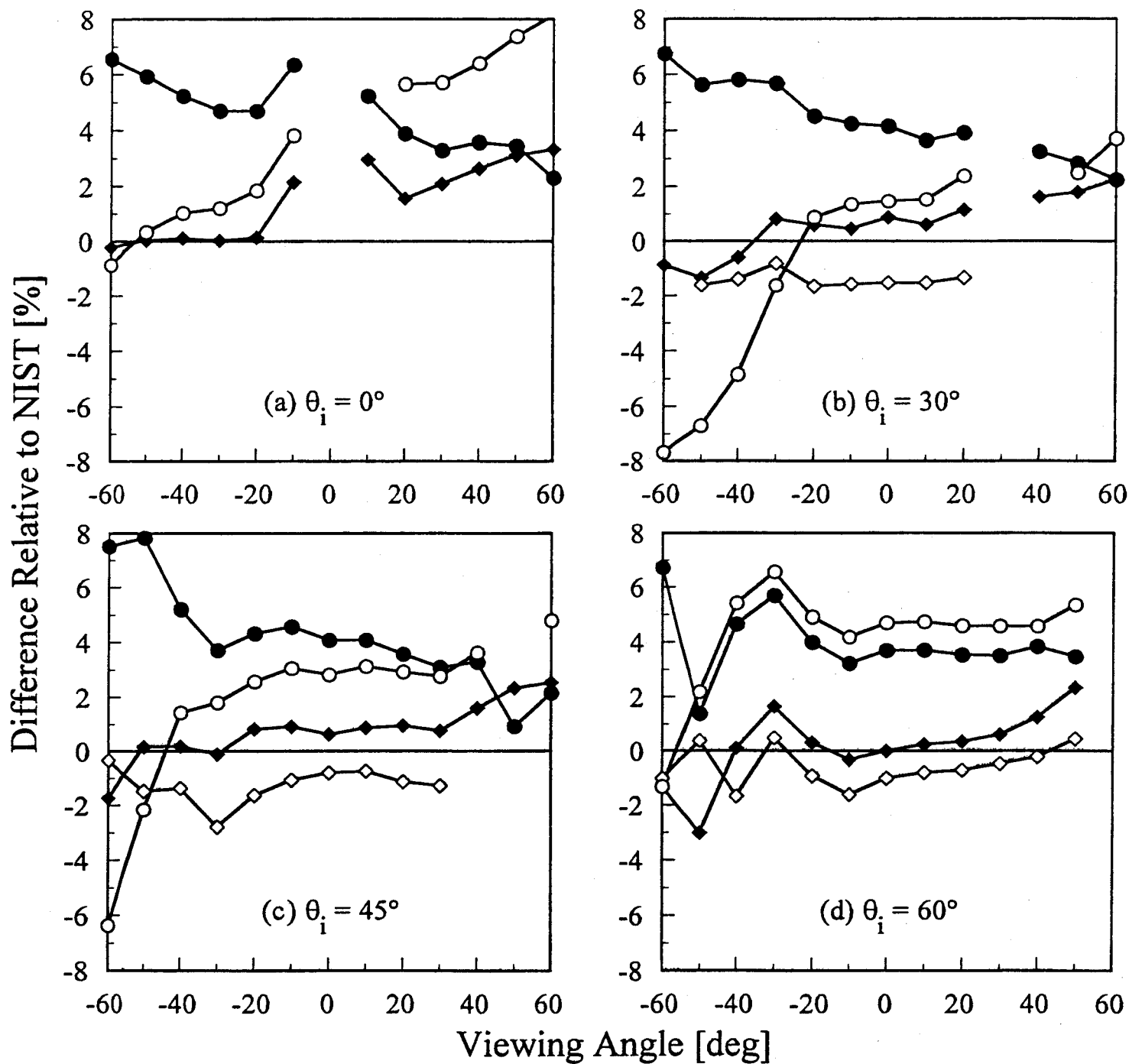


Figure 16

sintered PTFE,  $\lambda = 633$  nm

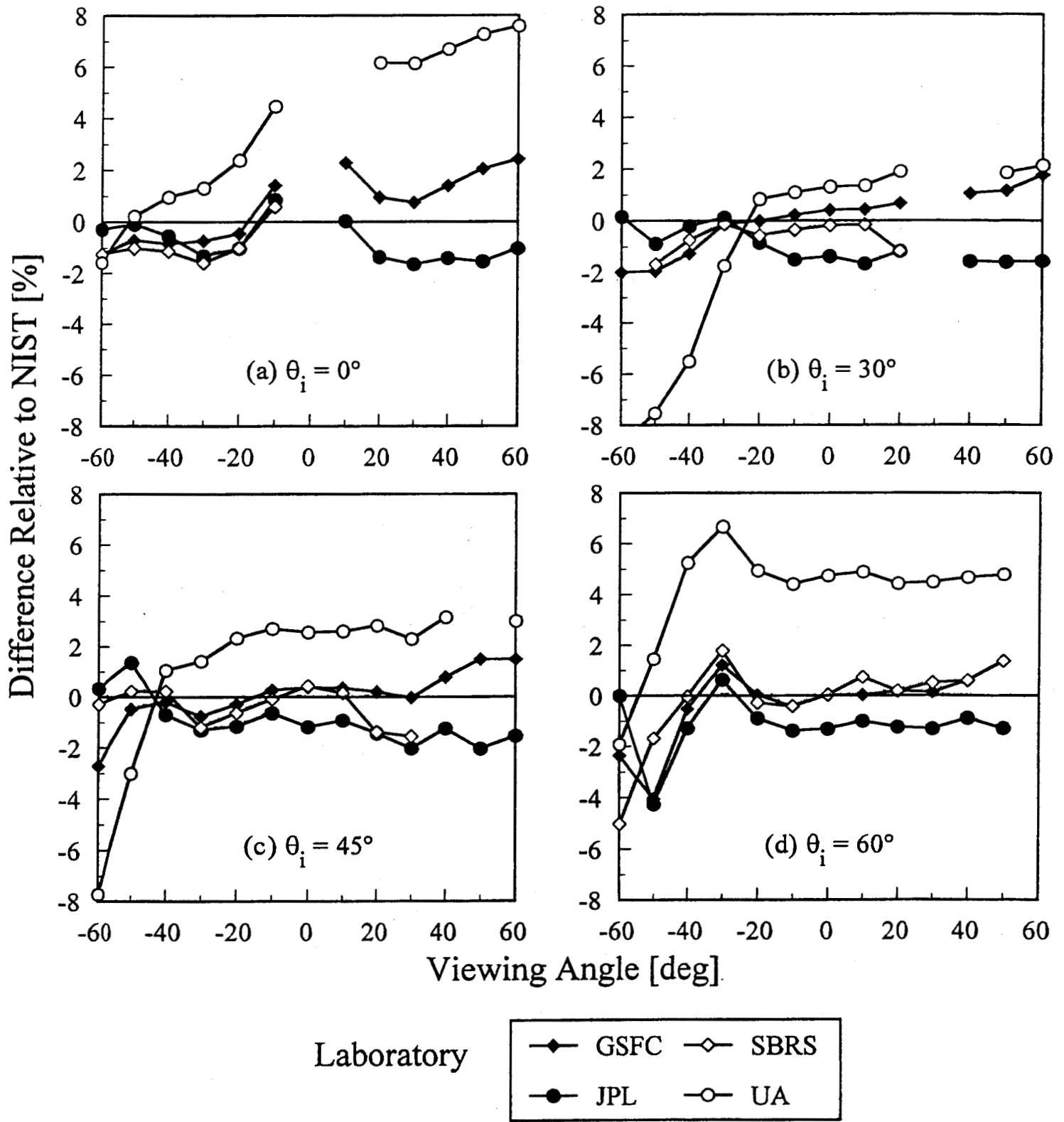


Figure 17

sintered PTFE,  $\lambda = 860$  nm

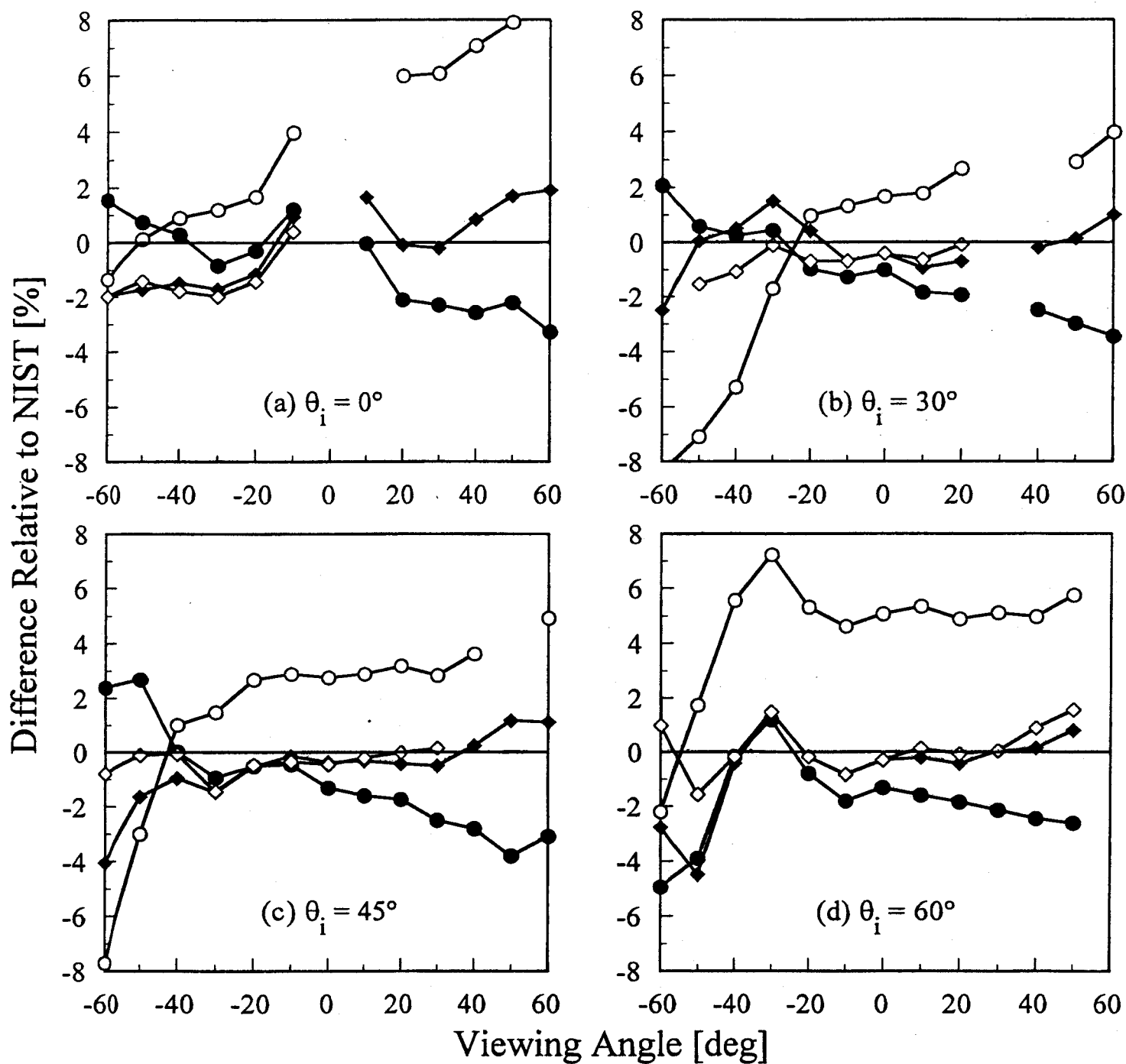
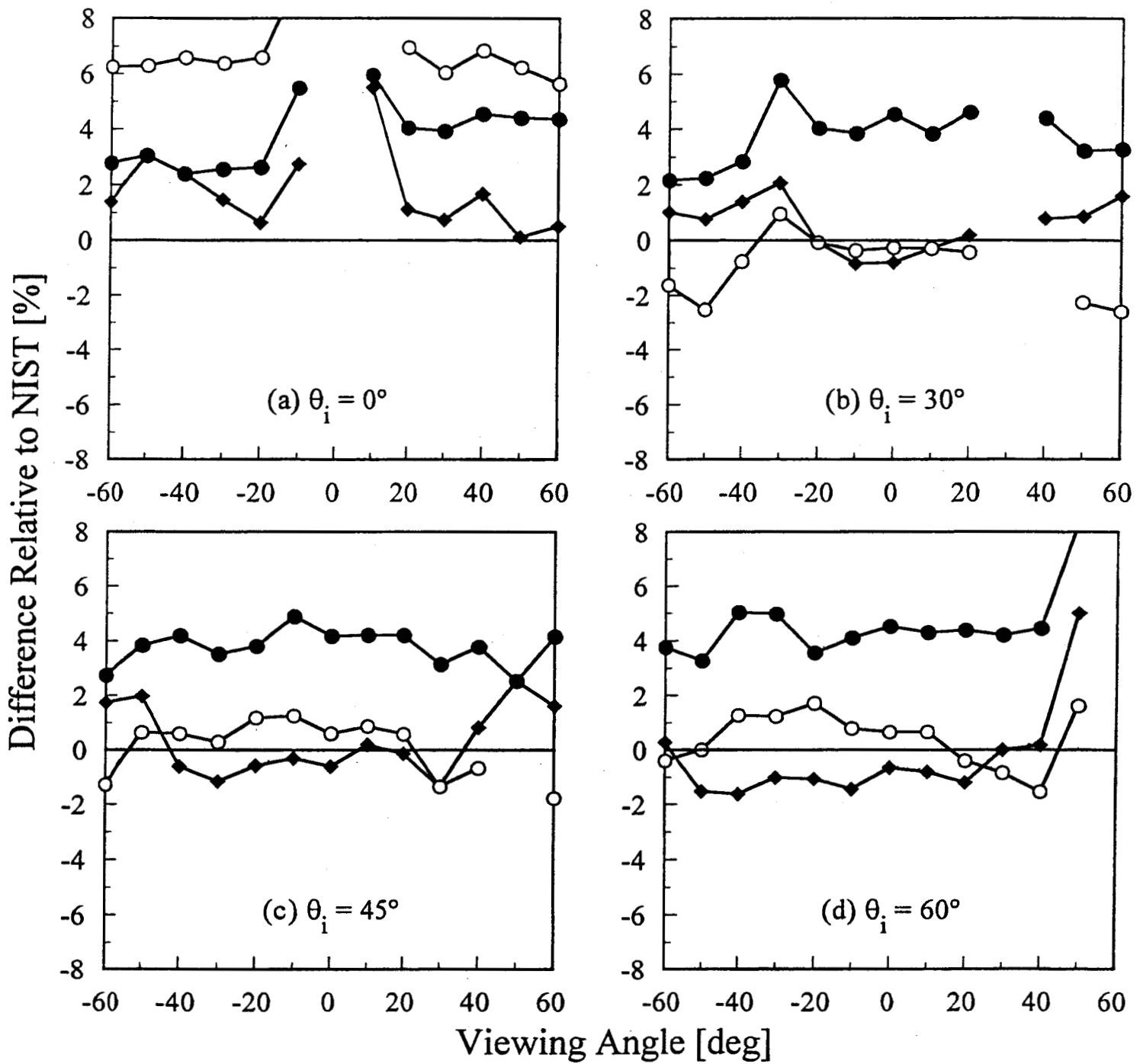


Figure 18

Aluminum,  $\lambda = 440$  nm



Laboratory

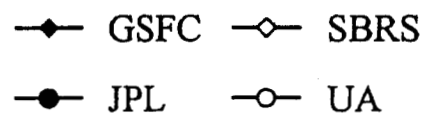


Figure 19

Aluminum,  $\lambda = 633 \text{ nm}$

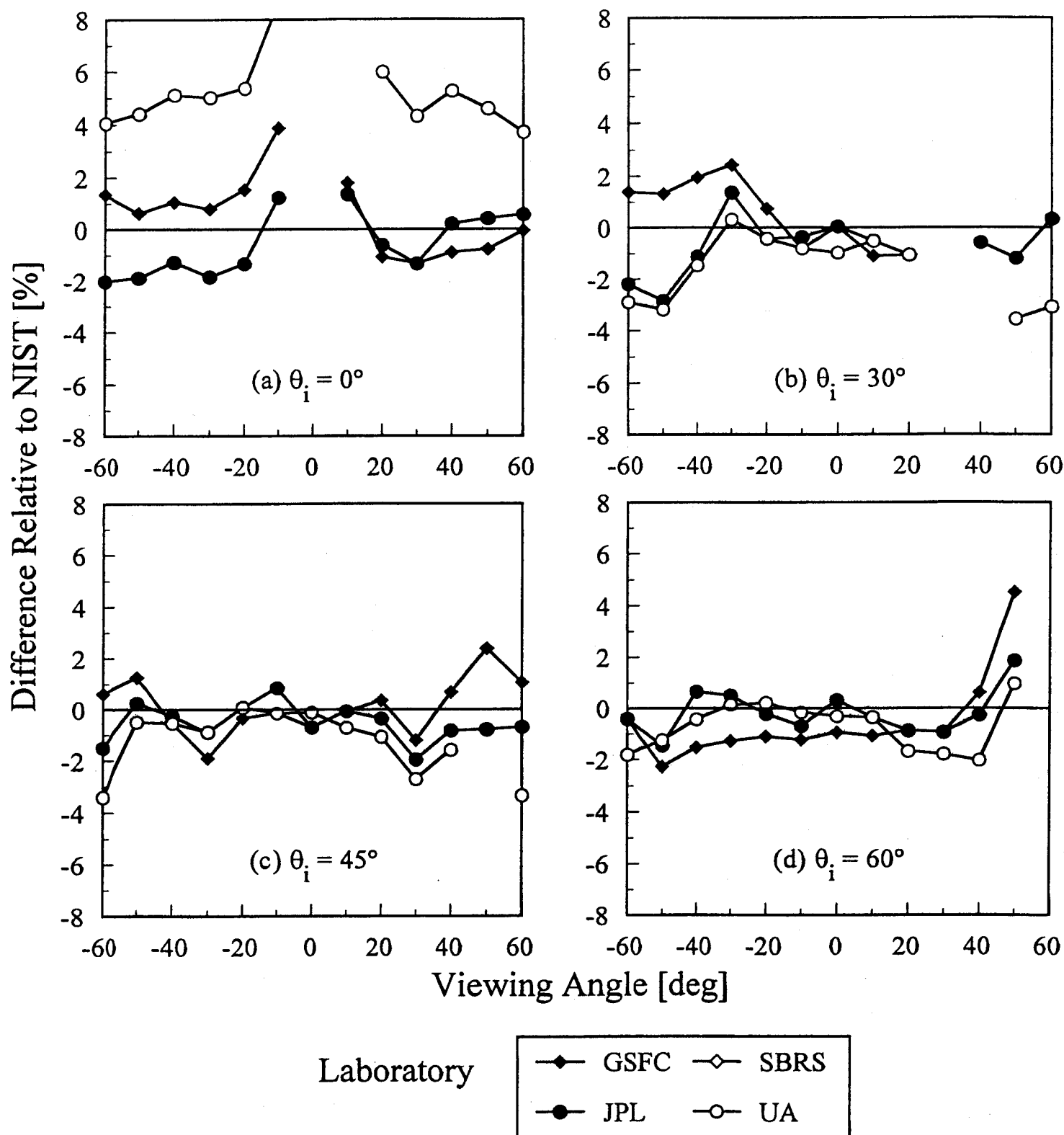


Figure 20

Aluminum,  $\lambda = 860 \text{ nm}$

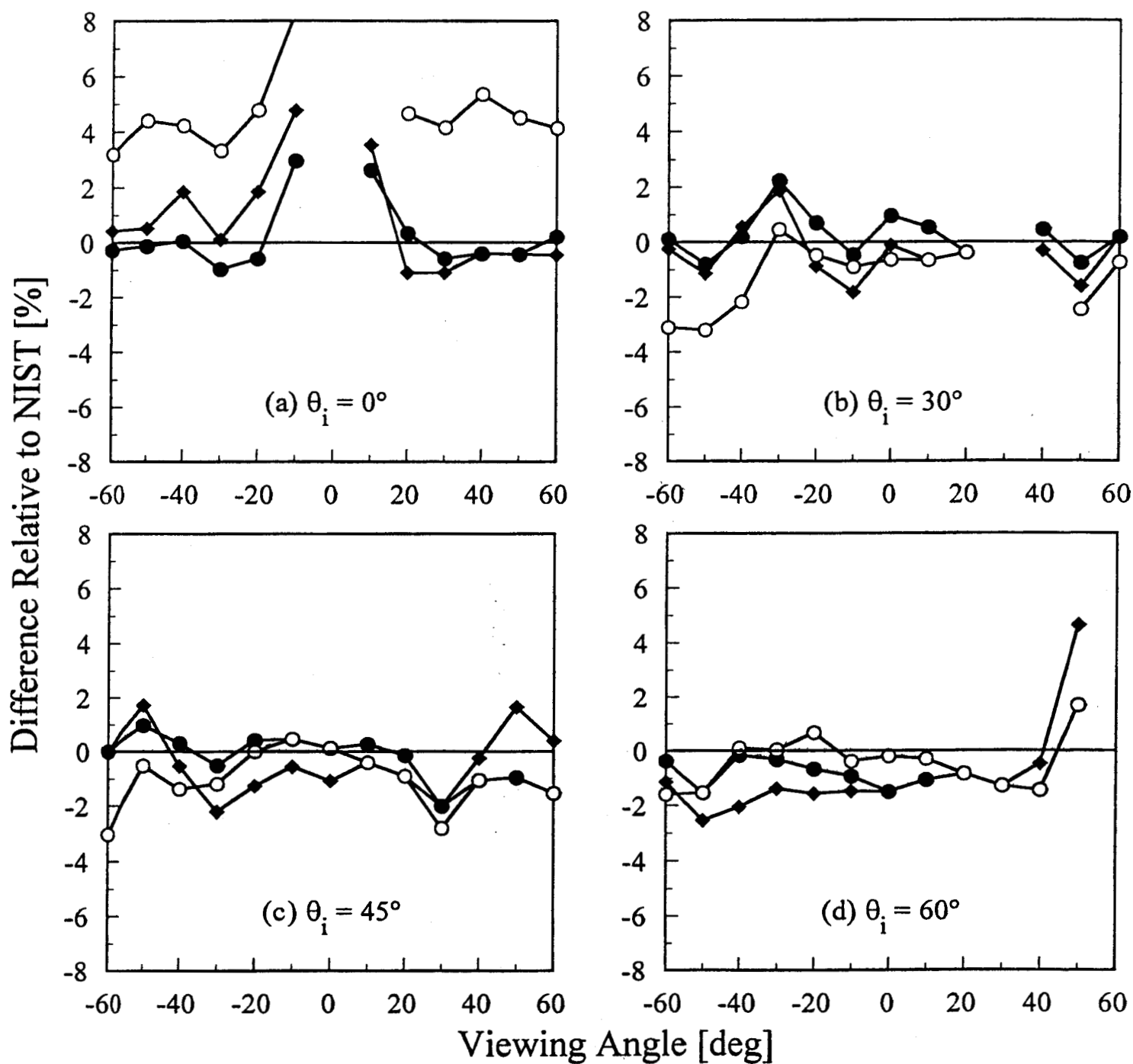


Figure 21

# GSFC

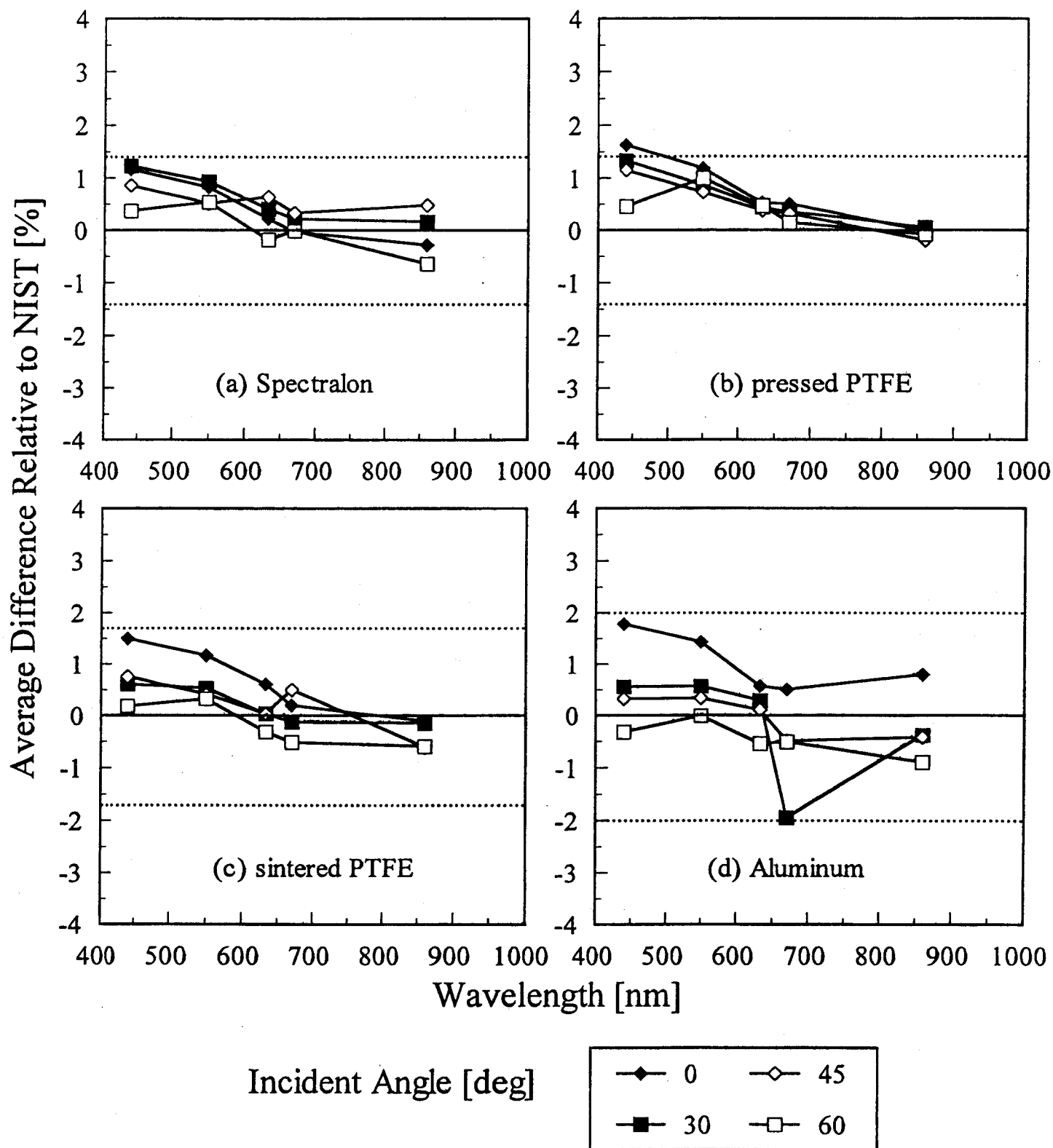


Figure 22

JPL

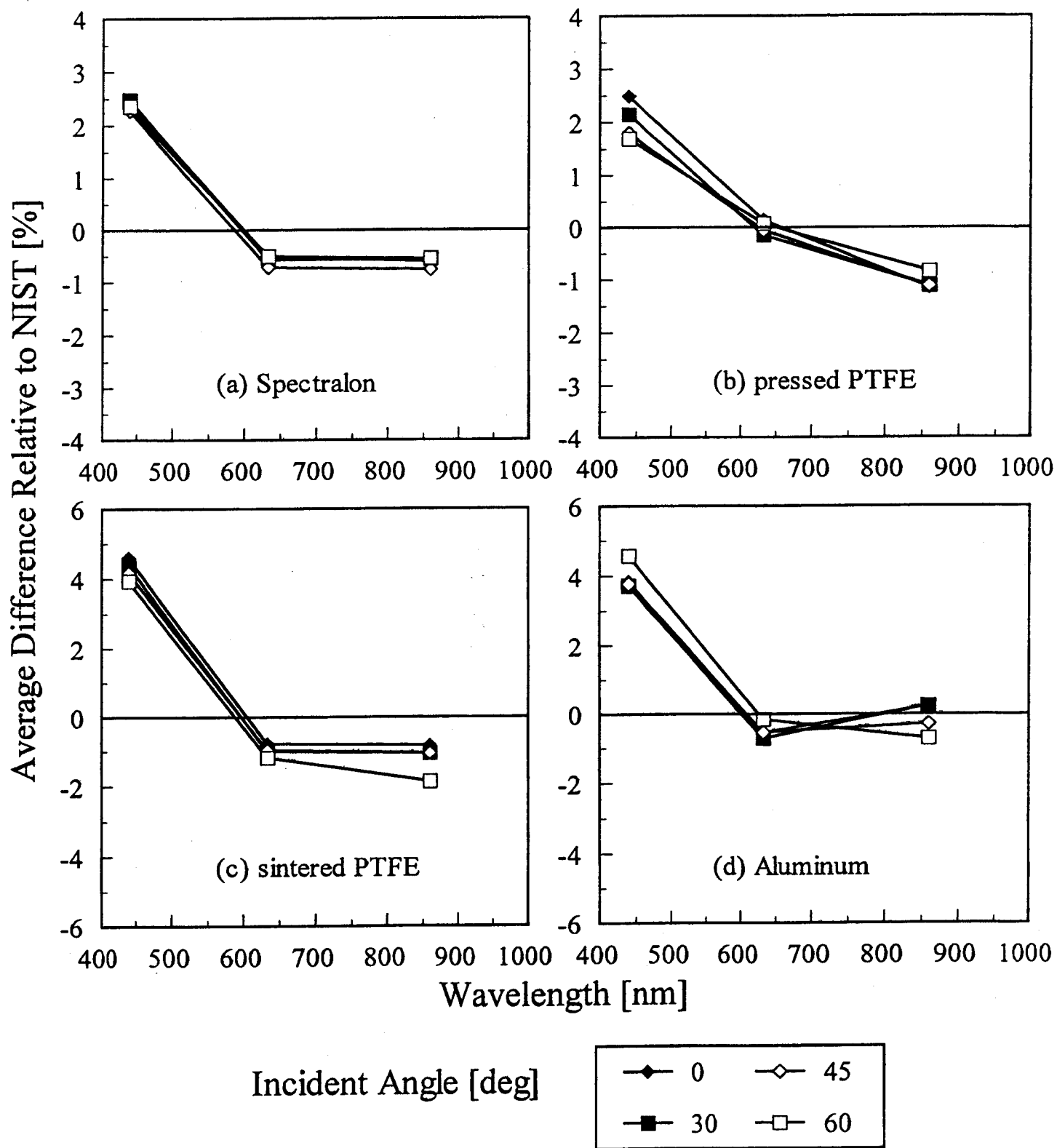
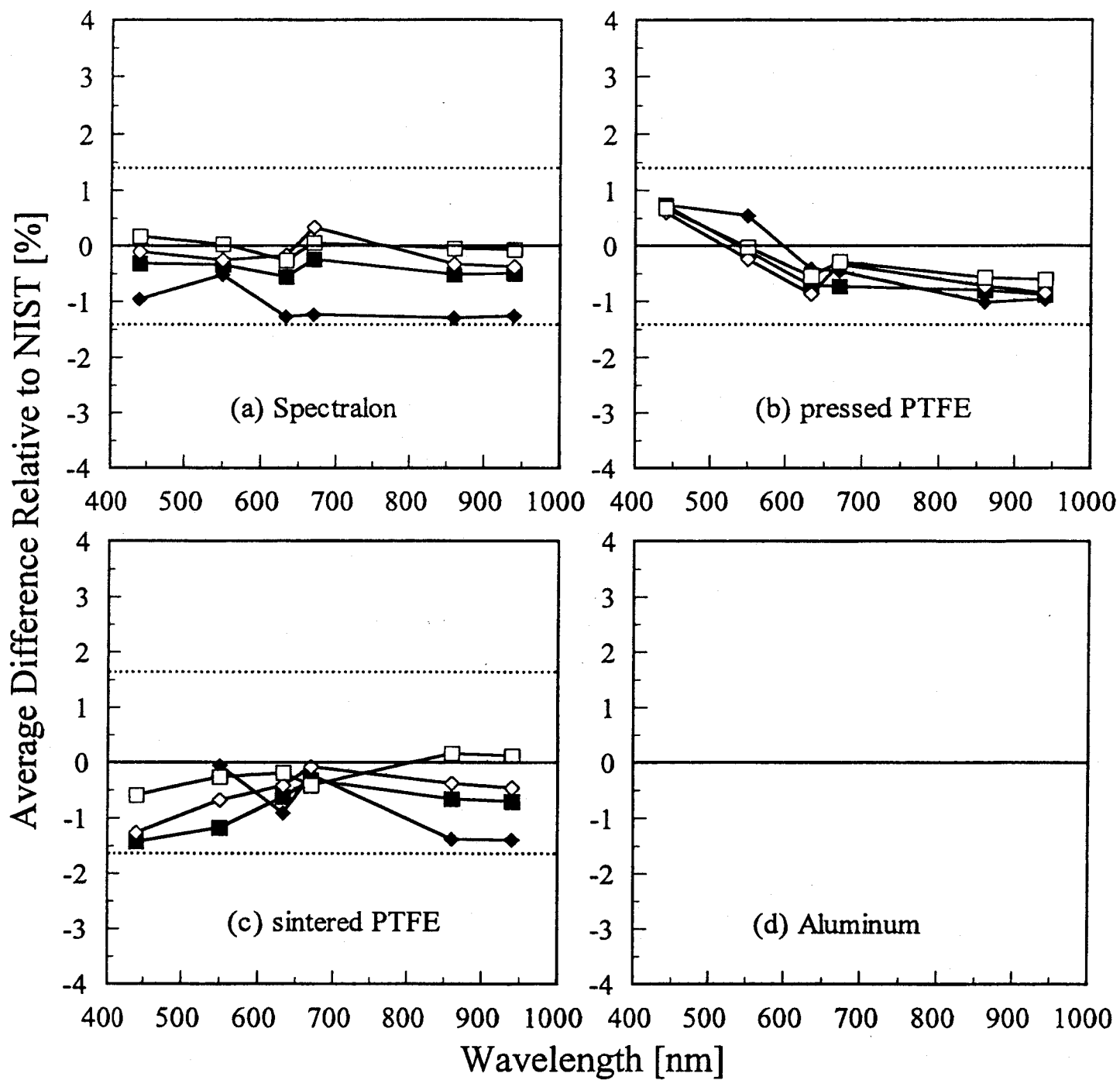


Figure 23

# SBRS



Incident Angle [deg]

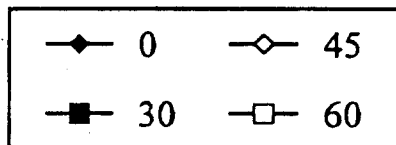


Figure 24

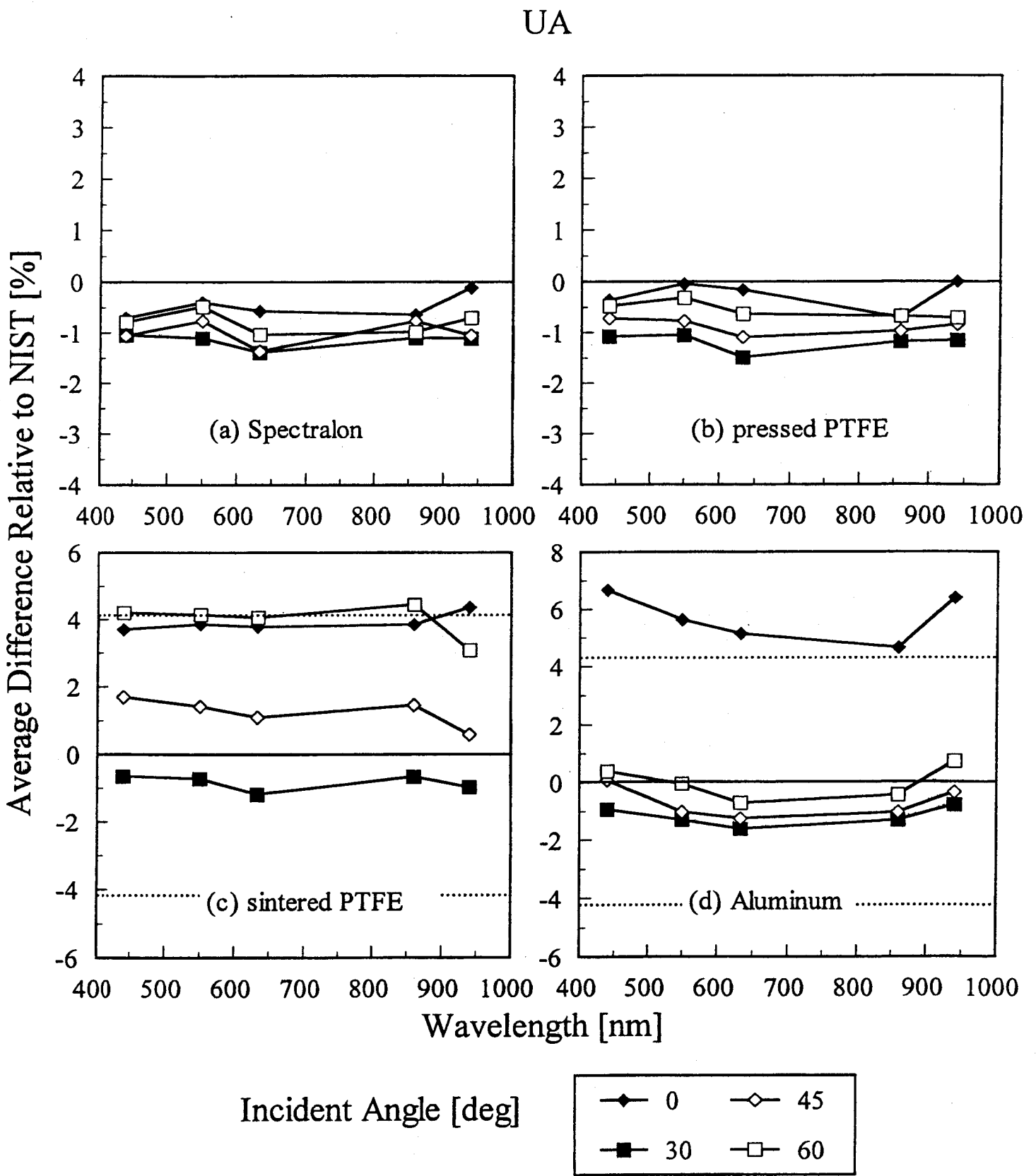


Figure 25

Spectralon,  $\lambda = 440$  nm

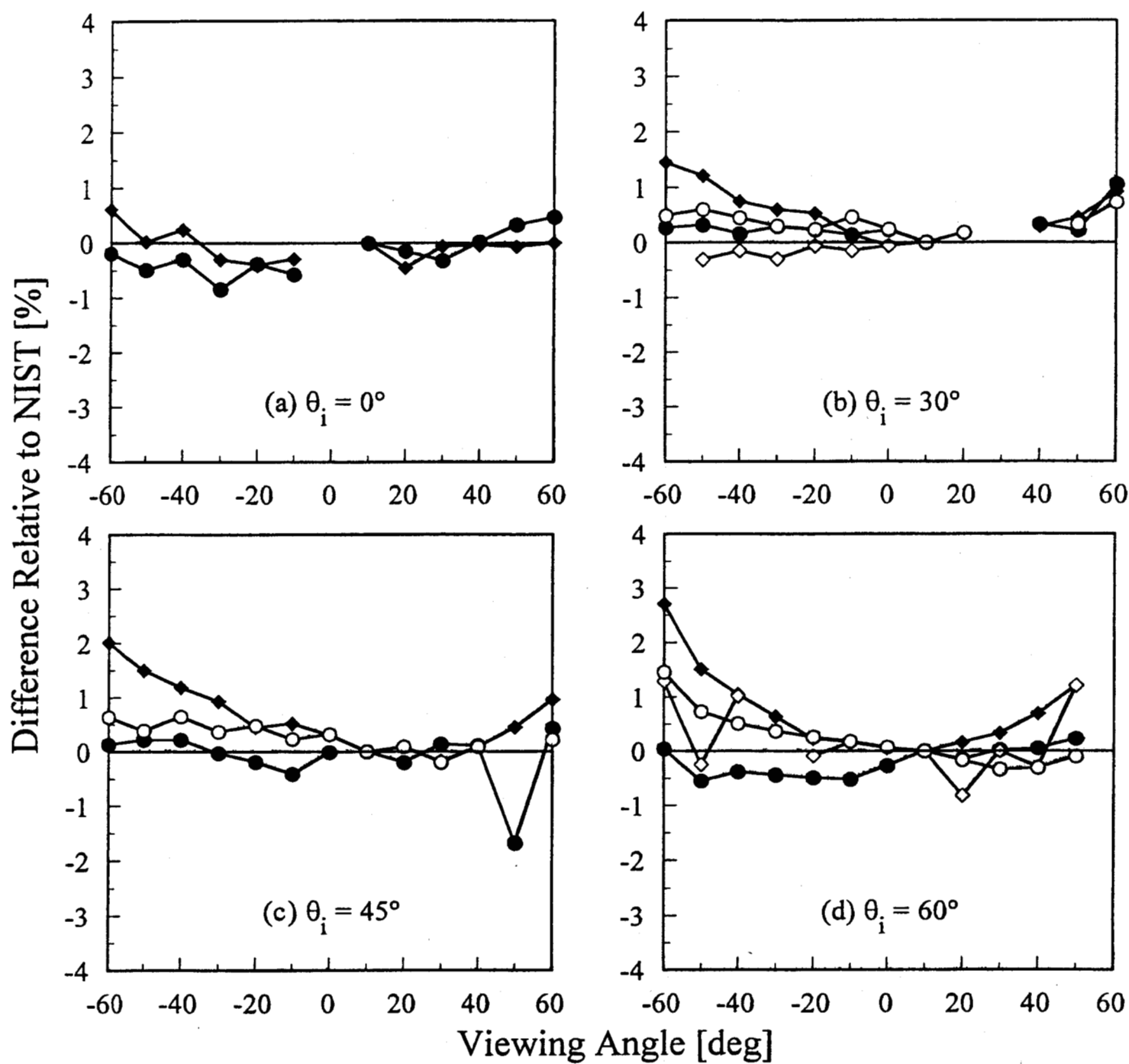


Figure 26

Spectralon,  $\lambda = 633$  nm

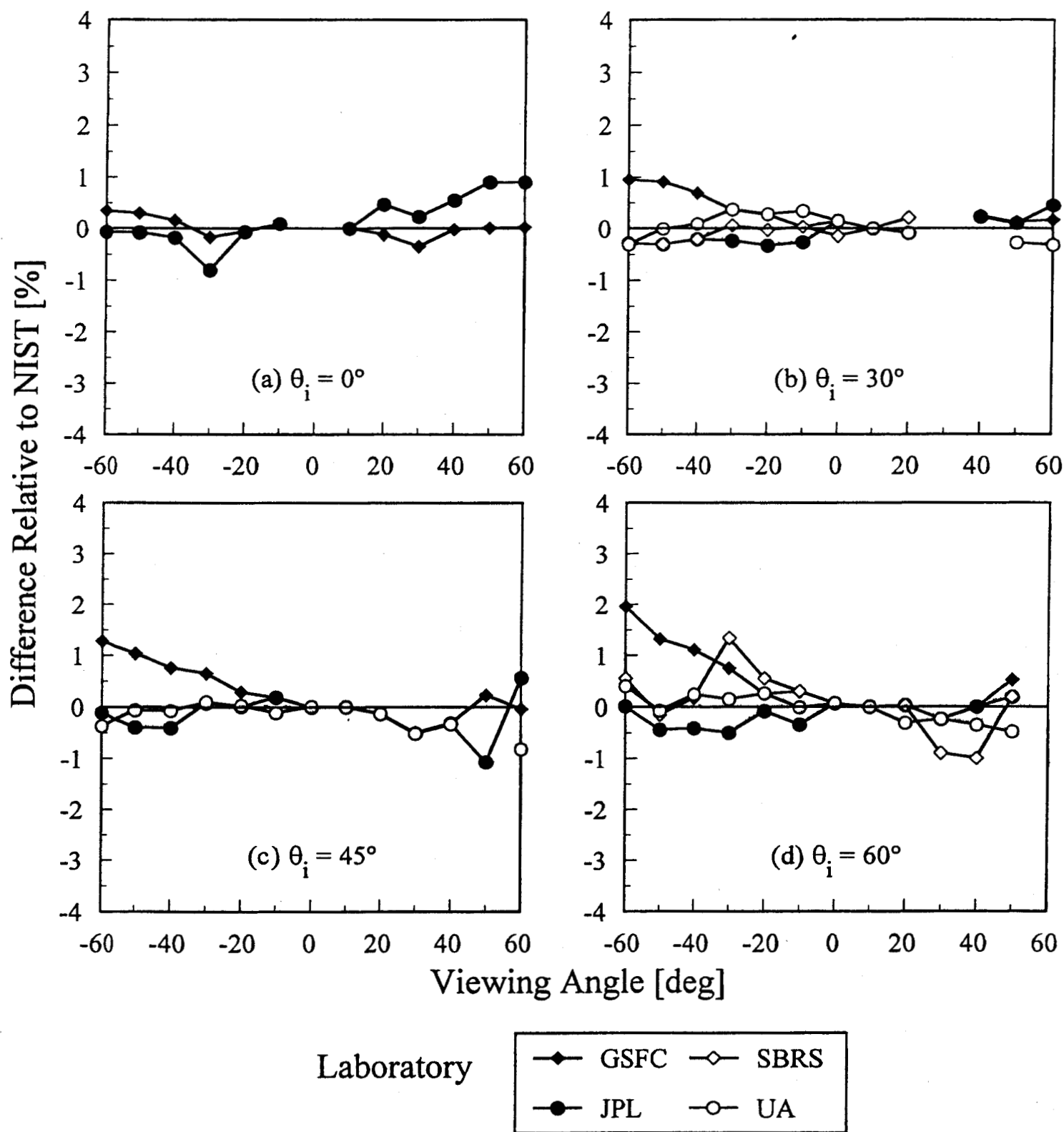


Figure 27

Spectralon,  $\lambda = 860 \text{ nm}$

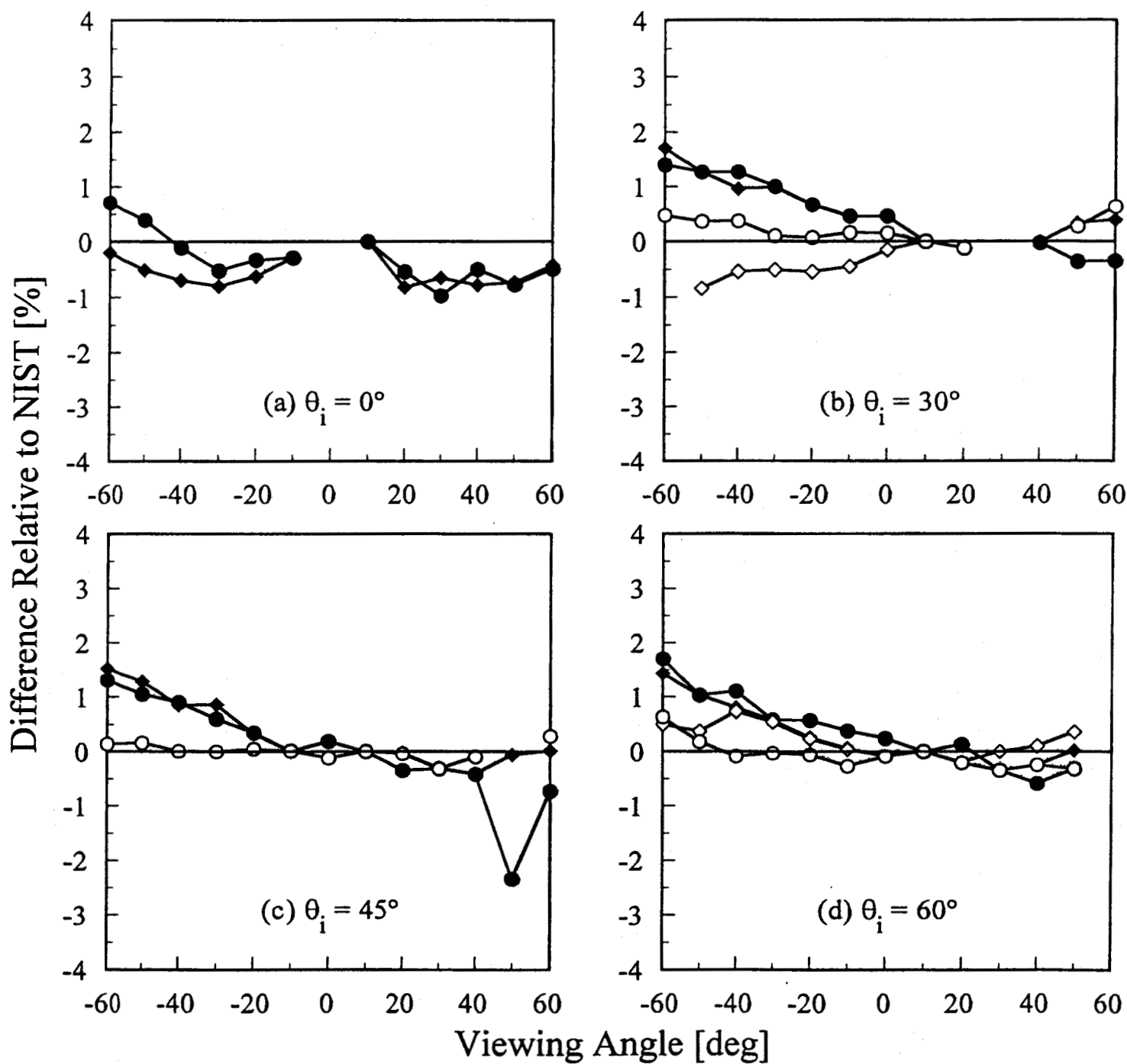


Figure 28

# Spectralon

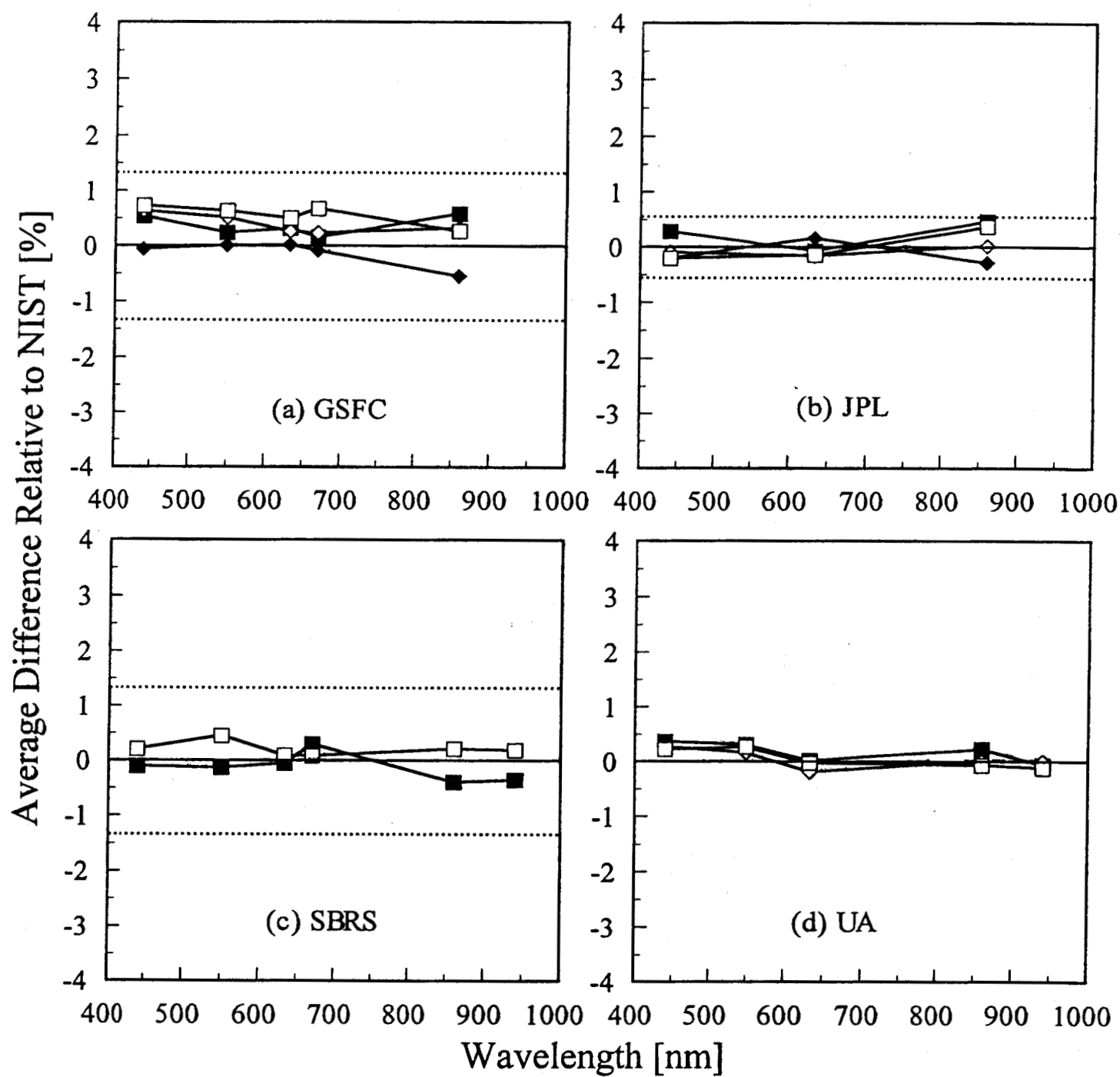


Figure 29